Contribution of Impaired Myocardial Insulin Signaling to Mitochondrial Dysfunction and Oxidative Stress in the Heart

Sihem Boudina, PhD; Heiko Bugger, MD, PhD; Sandra Sena, PhD; Brian T. O'Neill, MD, PhD; Vlad G. Zaha, MD, PhD; Olesya Ilkun, MS; Jordan J. Wright, BS; Pradip K. Mazumder, DVM, PhD; Eric Palfreyman, MD; Timothy J. Tidwell; Heather Theobald, BS; Oleh Khalimonchuk, PhD; Benjamin Wayment, BS; Xiaoming Sheng, PhD; Kenneth J. Rodnick, PhD; Ryan Centini, BS; Dong Chen, PhD; Sheldon E. Litwin, MD; Bart E. Weimer, PhD; E. Dale Abel, MBBS, DPhil

Background**—**Diabetes-associated cardiac dysfunction is associated with mitochondrial dysfunction and oxidative stress, which may contribute to left ventricular dysfunction. The contribution of altered myocardial insulin action, independent of associated changes in systemic metabolism, is incompletely understood. The present study tested the hypothesis that perinatal loss of insulin signaling in the heart impairs mitochondrial function.

Methods and Results**—**In 8-week-old mice with cardiomyocyte deletion of insulin receptors (CIRKO), inotropic reserves were reduced, and mitochondria manifested respiratory defects for pyruvate that was associated with proportionate reductions in catalytic subunits of pyruvate dehydrogenase. Progressive age-dependent defects in oxygen consumption and ATP synthesis with the substrate glutamate and the fatty acid derivative palmitoyl-carnitine were observed. Mitochondria also were uncoupled when exposed to palmitoyl-carnitine, in part as a result of increased reactive oxygen species production and oxidative stress. Although proteomic and genomic approaches revealed a reduction in subsets of genes and proteins related to oxidative phosphorylation, no reductions in maximal activities of mitochondrial electron transport chain complexes were found. However, a disproportionate reduction in tricarboxylic acid cycle and fatty acid oxidation proteins in mitochondria suggests that defects in fatty acid and pyruvate metabolism and tricarboxylic acid flux may explain the mitochondrial dysfunction observed.

Conclusions**—**Impaired myocardial insulin signaling promotes oxidative stress and mitochondrial uncoupling, which, together with reduced tricarboxylic acid and fatty acid oxidative capacity, impairs mitochondrial energetics. This study identifies specific contributions of impaired insulin action to mitochondrial dysfunction in the heart. **(*Circulation*. 2009;119:1272-1283.)**

Key Words: insulin ■ metabolism ■ mitochondria ■ oxidative stress

Recent studies have suggested that impaired mitochondrial energetics may contribute to cardiac dysfunction in obesity and diabetes mellitus.[1–7] The pathogenesis of mitochondrial dysfunction in obesity or diabetes-related heart disease is likely multifactorial but includes fatty acid (FA)–mediated mitochondrial uncoupling and oxidative damage.[3,4,8–11] A commonly associated finding in the heart in experimental models of obesity and diabetes mellitus is myocardial insulin resistance.[12–16] However, it is not known whether myocardial insulin resistance per se contributes directly to the pathogenesis of myocardial mitochondrial dysfunction.

Clinical Perspective p 1283

The effects of myocardial insulin signaling on the acute regulation of myocardial metabolism are well known[17,18] and include increasing glucose uptake and glycolysis via regulation of GLUT4 translocation[19,20] and activation of 6-phosphofructo-1-kinase.[21] In perfused hearts, insulin increases glucose oxidation and reduces FA oxidation.[13] In vivo, the antilipolytic effect of insulin also reduces the delivery of free FAs to the heart, which further reduces myocardial FA oxidation.[18] The direct effects of reduced insulin signaling on myocardial

Received September 20, 2007; accepted January 6, 2009.

From the Division of Endocrinology, Metabolism and Diabetes and Program in Molecular Medicine (S.B., H.B., S.S., B.T.O., V.G.Z., O.I., J.J.W., P.K.M., E.P., T.J.T., H.T., E.D.A.), Department of Biochemistry (O.K., E.D.A.), Division of Cardiology (B.W., S.E.L.), and Department of Family and Preventive Medicine (X.S.), University of Utah School of Medicine, Salt Lake City; Department of Biological Sciences, Idaho State University, Pocatello (K.J.R.); and Center for Integrated BioSystems, Utah State University, Logan (R.C., D.C., B.E.W.).

The online-only Data Supplement can be found with this article at http://circ.ahajournals.org/cgi/content/full/CIRCULATIONAHA.108.792101/DC1.

Correspondence to E. Dale Abel, Division of Endocrinology, Metabolism and Diabetes, Program in Molecular Medicine, 15 N 2030 E Bldg No. 533, Room 3110B, Salt Lake City, Utah 84112. E-mail dale.abel@hmbg.utah.edu

***Circulation* is available at http://circ.ahajournals.org** **DOI: 10.1161/CIRCULATIONAHA.108.792101**

substrate use are not well understood, in part because systemic insulin deficiency or insulin resistance increases the delivery of FA to the heart in vivo, which increases myocardial FA use and activates peroxisome proliferator-activated receptor-α–mediated transcriptional pathways that further augment myocardial FA oxidative capacity.[22] In contrast, perinatal loss of insulin receptors in cardiomyocytes reduces myocardial glucose and FA oxidation,[23] suggesting that the direct effect of insulin deficiency on myocardial substrate use is distinct from effects that are secondary to loss of insulin signaling in the periphery.

The present study sought to elucidate the direct effects of impaired insulin action on cardiac mitochondria in the absence of systemic metabolic disturbances that accompany insulin resistance or insulin deficiency. Thus, we examined mitochondrial function in mice with perinatal loss of insulin receptors in cardiomyocytes (CIRKO) to test the hypothesis that impaired myocardial insulin action might contribute to mitochondrial dysfunction in the heart in insulin-resistant states. This study demonstrates that genetic deletion of insulin receptors in cardiomyocytes impairs mitochondrial function via multiple mechanisms that include loss of tricarboxylic acid (TCA) cycle and β-oxidation proteins, oxidative stress, and mitochondrial uncoupling. Thus, impaired myocardial insulin signaling might directly contribute to mitochondrial dysfunction in conditions such as obesity and diabetes mellitus.

Methods

Generation of Mice

Mice with cardiomyocyte-selective ablation of the insulin receptor (CIRKO), generated as previously described,[23] were fed standard chow (see Materials in the online-only Data Supplement for composition of chow) and housed in temperature-controlled facilities with a 12-hour light/dark cycle (lights on at 6 AM). Animals were studied in the random-fed state during the day (between 7 AM and 1 PM) using protocols approved by the Institutional Animal Care and Use Committee of the University of Utah.

Determination of Cardiac Function by Echocardiography

Echocardiography was performed in lightly anesthetized (isoflurane) mice with a Vivid7 echocardiogram unit (General Electric, Tampa, Fla) by an investigator blinded to genotype and analyzed as previously described.[23–25]

Cardiac Function MV_{O_2} and Substrate Use in Perfused Mouse Hearts

Retrograde heart perfusions were performed in 8-, 24-, and 54-week-old mice as previously described[3] with Krebs buffer containing (in mmol/L) 118 NaCl, 4.7 KCl, 25 $NaHCO_3$, 1.2 $MgSO_4$, 1.2 KH_2PO_4, 2 $CaCl_2$, and 11 glucose gassed with 95% O_2 and 5% CO_2. Heart rates were maintained at 360 bpm by pacing at 6 Hz at the level of the atria. Oxygen consumption was calculated as previously described.[3] Eight-week-old mouse hearts also were subjected to calcium-induced inotropic stress using our previously described protocols.[3] Palmitate oxidation rates and MV_{O_2} were determined in isolated working hearts as previously described.[13]

Mitochondrial Respiration and ATP Synthesis

Mitochondrial function (oxygen consumption and ATP synthesis rates) were studied in saponin-permeabilized fibers as described[3,4,26] and in mitochondria isolated by differential centrifugation[27] (see online-only Data Supplement Methods). Substrates used were 5 mmol/L glutamate and 2 mmol/L malate, 10 mmol/L pyruvate and 5 mmol/L malate, or 20 μmol/L palmitoyl-carnitine (PC) with 2 mmol/L malate. To evaluate maximal respiratory capacity of isolated mitochondria, O_2 consumption was determined in pyruvate-exposed mitochondria after treatment with oligomycin (1 μg/mL) and the addition of carbonyl cyanide p-trifluoromethoxyphenylhydrazone (FCCP; 0.7 μmol/L).

Mitochondrial Fractionation

Isolated mitochondria were resuspended in 100 μL of 10 mmol/L Tris/HCl (pH 8.5) and subjected to 3 freeze-thaw cycles with liquid nitrogen. Lysed mitochondria were centrifuged twice at 40 000g for 20 minutes at 4°C. The supernatant (matrix fraction) and the pellet (membrane fraction) were stored/suspended in 10 mmol/L Tris/HCl and maintained at −80°C until used for proteomic analysis by mass spectroscopy or blue-native PAGE (membranes only). The fractionation protocol yields a matrix fraction and a membrane fraction (containing outer and inner mitochondrial membranes) that are enriched for respective representative proteins with minimal cross-contamination (online-only Data Supplement Figure I).

Blue-Native Gel Electrophoresis and In-Gel Complex Activities

Blue-native PAGE was performed as described,[28] with some modifications (see online-only Data Supplement Methods).

Mitochondrial Proteomics by Mass Spectrometry

Differentially expressed mitochondrial matrix and membrane proteins were identified with liquid chromatography and mass spectroscopy. Samples were initially subjected to tryptic digestion before liquid chromatography and parallel fragmentation mass spectroscopy (see online-only Data Supplement Methods).

Hydrogen Peroxide Measurement

Mitochondrial hydrogen peroxide (H_2O_2) generation was measured as previously described[4] except that PC 60 μmol/L and L-carnitine 2 mmol/L were used as substrates.

Treatment of Mice With the Antioxidant MnTBAP

Four groups of mice were treated starting at 4 weeks of age. Wild-type and CIRKO mice (n=12 per group) received twice-weekly intraperitoneal injections (20 mg/kg body weight) of the cell-permeable superoxide dismutase mimetic and peroxynitrite scavenger MnTBAP [Mn (III) tetrakis (4-benzoic acid) porphyrin chloride; EMD Chemicals Inc, San Diego, Calif] for 4 weeks. Control wild-type and CIRKO mice (n=12 per group) received twice-weekly intraperitoneal injections of saline. After treatment, animals were euthanized and hearts were collected for determination of aconitase activity and oligomycin-insensitive respiration rates.

Western Blot Analysis

Western blot analysis was performed with total heart or mitochondrial proteins as previously described (see online-only Data Supplement Methods).[3]

Gene Expression

Total RNA was extracted from ≈30 mg heart tissue with Trizol reagent (Invitrogen Corp, Carlsbad, Calif) and purified with the RNEasy Kit (Qiagen Inc, Valencia, Calif). Equal amounts of heart RNA from 6 mice were subjected to real-time polymerase chain reaction with an ABI Prism 7900HT instrument (Applied Biosystems, Foster City, Calif) in 384-well plate format with SYBR Green I chemistry and ROX internal reference (Invitrogen) as previously described.[4,25] All reactions were performed in triplicate. Data were normalized to cyclophilin. See online-only Data Supplement Table I for primer sequences.

Table 1. In Vivo Cardiac Function Measured by Echocardiography

	27 Weeks of Age		67 Weeks of Age	
	Wild Type (n=7)	CIRKO (n=8)	Wild Type (n=5)	CIRKO (n=5)
LVDd, cm*	0.39±0.01	0.39±0.007	0.42±0.01	0.41±0.01
LVDs, cm	0.27±0.01	0.30±0.008	0.31±0.02	0.31±0.006
IVSd, cm†	0.08±0.004	0.07±0.003	0.08±0.005	0.07±0.003
IVSs, cm	0.10±0.01	0.10±0.003	0.12±0.008	0.10±0.005
PWd, cm	0.08±0.006	0.07±0.003	0.08±0.004	0.07±0.003
PWs, cm	0.11±0.004	0.10±0.003	0.11±0.007	0.10±0.003
FS, %†	29.40±1.75	24.43±0.91	25.95±2.49	24.09±1.3
EF†	0.64±0.02	0.56±0.01	0.58±0.04	0.56±0.02
HR, bpm	455±31	474±15	460±16	443±23
SV, mL	0.03±0.003	0.03±0.002	0.04±0.003	0.04±0.004
CO, mL/min	17.29±1.54	17.02±0.92	20.45±1.06	18.34±2.22

LVDd indicates left ventricular dimension in diastole; LVDs, left ventricular dimension in systole; IVSd, interventricular septum in diastole; IVSs, interventricular septum in systole; PWd, posterior wall of left ventricle in diastole; PWs, posterior wall of left ventricle in systole; FS, fractional shortening; EF, ejection fraction; HR, heart rate; SV, stroke volume; and CO, cardiac output. Values are mean±SEM.

*$P<0.05$, 27 versus 67 weeks (both genotypes respectively).

†$P<0.05$, wild type vs CIRKO (both ages) by 2-way ANOVA.

Electron Microscopy

Ventricular samples were analyzed by electron microscopy, and mitochondrial volume density and number were determined by stereology in a blinded fashion using the point counting method as previously described.[4,29] For volume density, 2 images per sample were analyzed (magnification ×2000) using 2 grids per image. For mitochondrial number, 3 images per sample were analyzed (magnification ×8000).

Statistical Analysis

Data are mean±SEM. Comparisons of a single variable in ≥2 age-matched groups were analyzed by 1-way ANOVA followed by Fisher least-protected-squares test (StatView 5.0.1 software, SAS Institute, Cary, NC). In analyses comparing ≥2 variables such as mitochondrial parameters in control and knockout mice as a function of age, a general linear model (eg, 2-way ANOVA) was used. When significant differences existed across multiple ages, a Tukey-Kramer multiple-comparison adjustment was performed on posthoc comparisons to determine at which ages the measures are different (SAS 9.0.3 software, SAS Institute). For all analyses, values of $P<0.05$ were considered significant. Unless specified, P values indicate statistically significant difference between groups across all ages. When differences (by posthoc analysis) exist between ages, they are indicated in the figure legends. Proteomic data were analyzed by the use of previously published algorithms.[30] In brief, the key algorithm in the Waters Protein Expression System is the clustering algorithm, which chemically clusters peptide components by mass and retention time for all injected samples and performs binary comparisons for each experimental condition to generate an average normalized intensity ratio for all matched accurate-mass, retention-time components. Student t test was used for each binary comparison.

The authors had full access to and take full responsibility for the integrity of the data. All authors have read and agree to the manuscript as written.

Results

Cardiac Function

Cardiac function was determined by echocardiography and in isolated hearts. We previously reported that fractional shortening and dP/dt (in vivo) were reduced by 20% and 30%, respectively, in 10-week-old CIRKO mice.[25] Thus, we determined in vivo cardiac function at later ages. Fractional shortening was reduced by 17% and 7% in CIRKO hearts relative to controls at 27 and 67 weeks of age, respectively (Table 1). In glucose-perfused Langendorff hearts, functional parameters declined with age in CIRKO and control hearts. However, developed pressure, rate-pressure product, and cardiac efficiency were always significantly reduced in CIRKO hearts at the 3 ages examined (8, 24, and 54 weeks; Table 2). Differences in cardiac function between 8-week-old CIRKO and control mice were accentuated under conditions

Table 2. Cardiac Function, MVo_2, and Cardiac Efficiency in Wild-Type and CIRKO Hearts Under Unstimulated Conditions

	8 Weeks of Age (n=17)		24 Weeks of Age (n=19)		54 Weeks of Age (n=7)	
	Wild Type	CIRKO	Wild Type	CIRKO	Wild Type	CIRKO
BW, g*	22.6±0.8	21.3±0.5	29.9±1.1	28.1±0.7	30.5±1.3	30.5±1.9
HW, g*†	0.14±0.01	0.10±0.03	0.16±0.01	0.12±0.01	0.17±0.05	0.15±0.02
HW/BW $\times10^3$†	6.1±0.2	4.7±0.11	5.3±0.12	4.2±0.15	5.4±0.1	4.8±0.3
HR, bpm	362±2	355±8	349±8	344±9	351±14	334±13
DP, mm Hg‡	12.1±1.5	12.9±1.7	9.6±1.0	10.5±1.2	15.4±2.3	14.3±1.8
SP, mm Hg*†	80.6±2.7	72.2±2.7	67±1.9	62.8±2.2	76.6±5.9	57.5±3.6
DVP, mm Hg*†	68.5±2.5	59.3±2.8	57.4±1.7	52.3±1.7	61.2±5.3	43.2±3.5
RPP $\times10^3$, mm Hg×bpm*†	24.8±0.9	21.1±1.2	20±0.6	18.1±0.8	21.2±1.6	14.2±0.8
−dP/dtmin $\times10^3$, mm Hg/s*	3.3±0.2	3.2±0.2	2.3±0.07	2.1±0.07	2.6±0.4	2.4±0.3
dP/dtmax $\times10^3$, mm Hg/s*	3.9±0.3	3.6±0.3	2.7±0.1	2.5±0.08	3.5±0.5	2.8±0.2
MVo_2, $\mu mol \cdot min^{-1} \cdot g^{-1}$	25.1±1.2	24.4±1.2	23.2±1.2	23.7±1.4	26±2.2	19.4±1.8
CE, %†	29.8±1.0	26±1.2	26.4±1.1	23.7±1.5	25.6±3.0	22.9±2.6

BW indicates body weight; HW, heart weight; HR, heart rate; DP, diastolic pressure; SP, systolic pressure; DVP, developed pressure; RPP, rate-pressure product; and CE, cardiac efficiency. Values are mean±SEM.

*Eight versus 24 and 54 weeks, $P<0.01$, 2-way ANOVA.

†Wild type versus CIRKO, $P<0.01$, 2-way ANOVA.

‡Twenty-four versus 54 weeks, $P<0.01$, 2-way ANOVA.

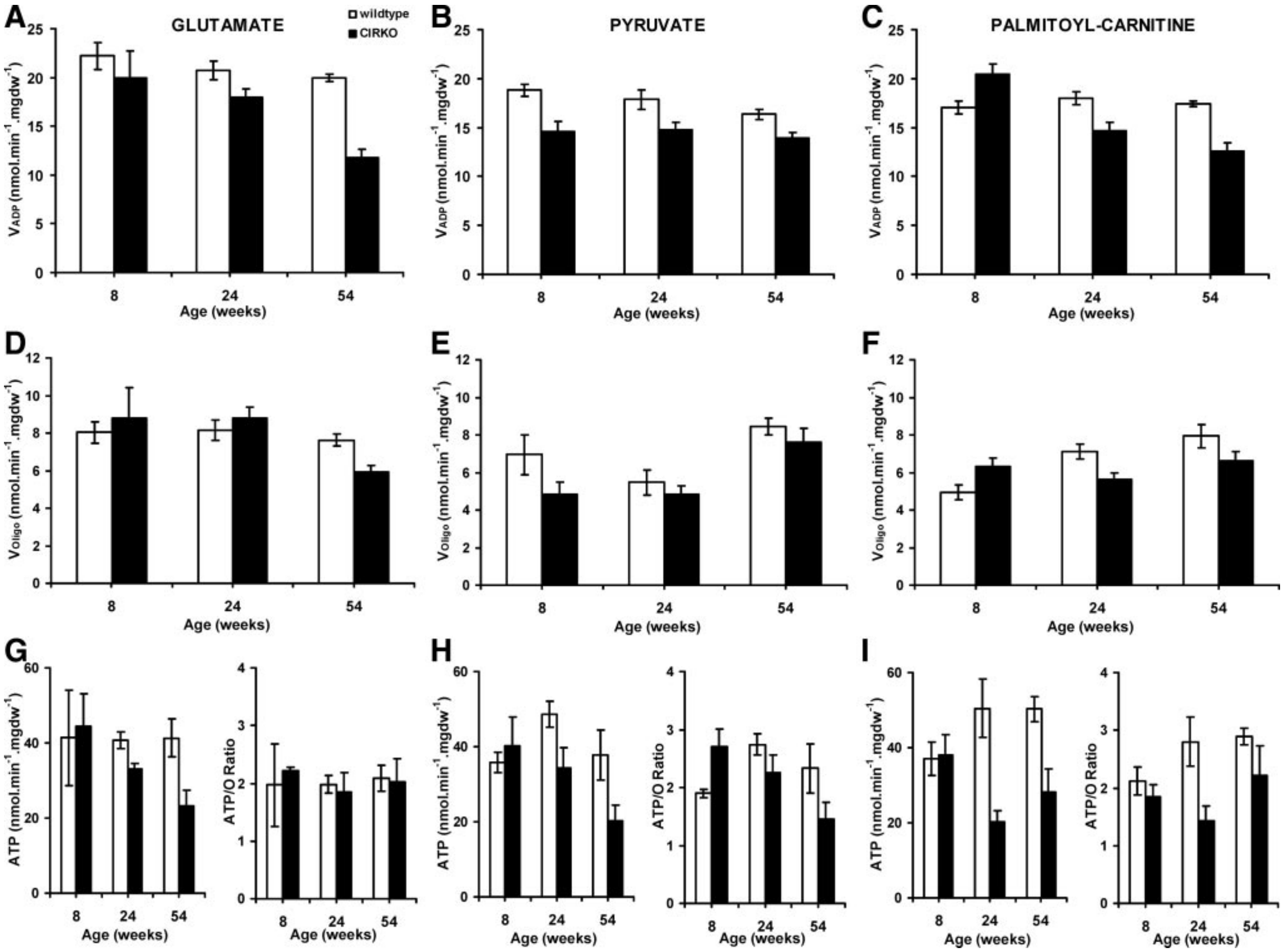

Figure 1. Age-dependent changes in mitochondrial respiration and ATP synthesis rates in CIRKO and wild-type mice. Data are mean±SEM. A, D, G, V_{ADP}, V_{Oligo}, ATP synthesis rates, and ATP/O ratio in the presence of glutamate-malate in 8- (n=4), 24- (n=4), and 54- (n=5) week-old CIRKO (black bars) and wild-type (WT) (white bars) mice, respectively. Statistics (2-way ANOVA): A, V_{ADP}—WT vs CIRKO, $P<0.01$; 54 vs 8 weeks, $P<0.01$; 24 vs 54 weeks, $P=0.06$. D, G, No statistical differences between groups. B, E, and H, Same as A, D, and G but in the presence of pyruvate-malate. Statistics (2-way ANOVA): B, V_{ADP}—WT vs CIRKO, $P<0.005$; E, V_{Oligo}—54 vs 24 or 8 weeks, $P<0.01$; H, ATP—WT vs CIRKO, $P<0.05$. C, F, and I, Same as A, D, and G but in the presence of PC and malate. Statistics (2-way ANOVA): C, V_{ADP}—WT vs CIRKO (at all ages), $P<0.05$; decline in CIRKO with age ($P<0.005$ after multiple comparison adjustments); F, V_{Oligo}—WT vs CIRKO (at 8 weeks), $P<0.005$; increase in WT with age ($P<0.005$ after multiple adjustments); I, ATP—WT vs CIRKO, $P<0.01$ and $P<0.05$ at 24 and 54 weeks, respectively; ATP/O—WT vs CIRKO, $P<0.01$.

of calcium-induced inotropic stress (online-only Data Supplement Figure II).

Mitochondrial Dysfunction in CIRKO Mice

Mitochondrial oxygen consumption and ATP production rates in cardiac fibers from 8-, 24-, and 54-week-old CIRKO mice were examined. With glutamate as substrate, maximal ADP-stimulated mitochondrial respirations (V_{ADP}) progressively declined with age (Figure 1A). At 8 weeks, CIRKO mice exhibited reduced V_{ADP} with pyruvate, which persisted up to 54 weeks and was associated with lower ATP synthesis rates in older animals (24 to 54 weeks; Figure 1B and 1H). With PC, V_{ADP} was initially increased in 8-week-old mice but declined progressively with age (Figure 1C). The increased PC respirations at 8 weeks were not associated with increased ATP synthesis rates (Figure 1I). By 24 weeks, ATP synthesis rates declined by 60% and the ATP/O ratio (ATP/V_{ADP}) declined by 50% compared with controls (Figure 1I). Thus, mitochondria from CIRKO hearts manifest 2 distinct functional defects: reduced respiratory capacity and ATP generation with all substrates and evidence for mitochondrial uncoupling (decreased ATP/O) when exposed to an FA substrate.

To confirm the existence of FA-induced mitochondrial uncoupling, studies with pyruvate- or PC-treated isolated mitochondria from 24-week-old mice were performed (Figure 2A through 2D and online-only Data Supplement Figure III). Respiration rates in isolated mitochondria are ≈10-fold higher than in permeabilized fibers. Under these conditions, the reduction in pyruvate respirations was no longer apparent in CIRKO mitochondria, and no differences were found in oligomycin-insensitive (V_{oligo}) respiration or respiratory control ratios. In contrast, in the presence of the FA substrate PC, V_{oligo} was increased by 1.3-fold, and the respiratory control ratio was proportionately reduced by 33%. Moreover, ATP and ATP/O ratios were reduced, supporting the existence of FA-induced mitochondrial uncoupling.

To determine whether reduced electron transport chain (ETC) function accounted for mitochondrial respiratory im-

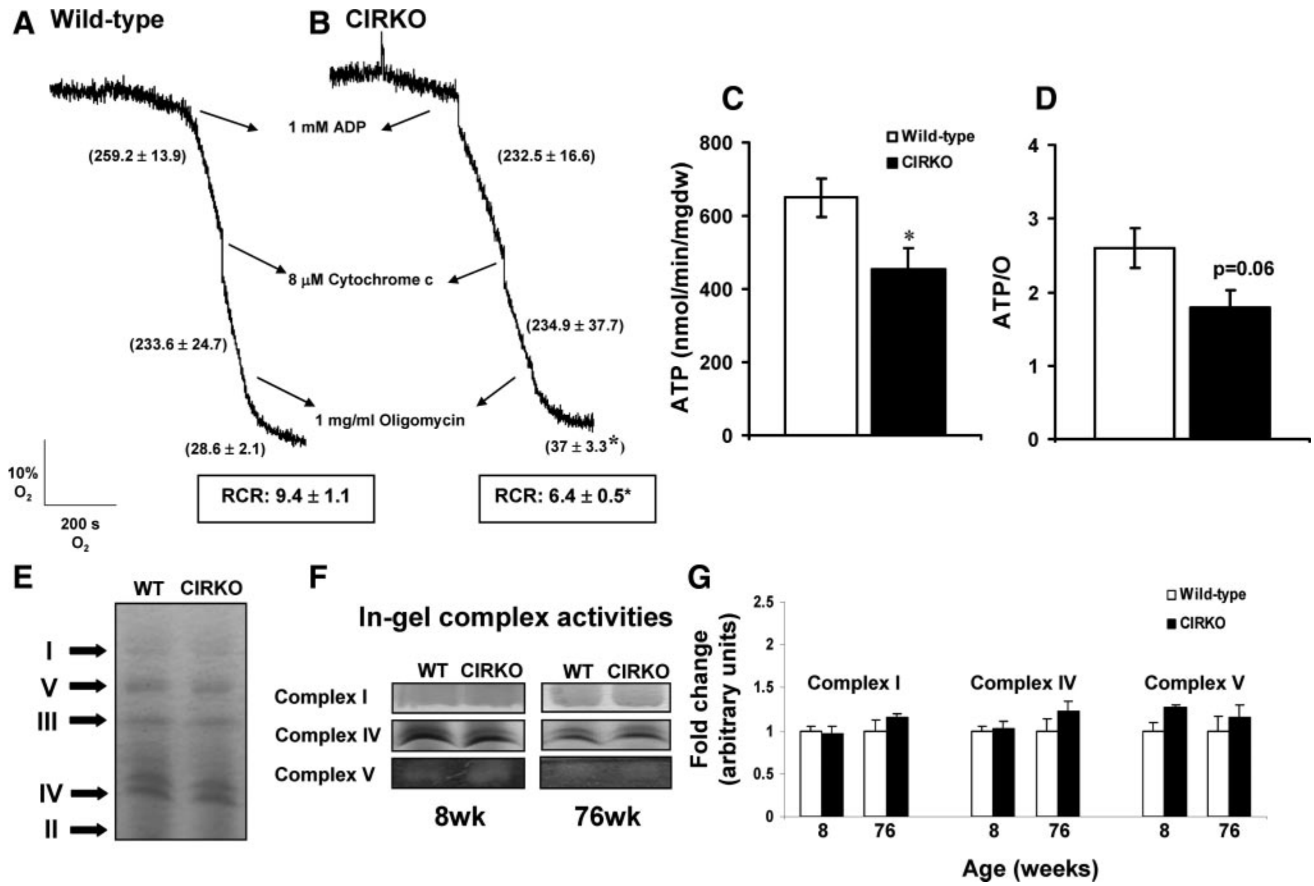

Figure 2. Mitochondrial function and ETC complex activity. A and B, Respiration traces of mitochondria (0.4 mg/mL) isolated from 24-week-old wild-type (n=5) and CIRKO mice (n=5), respectively, using PC as substrate. C and D, ATP and ATP/O ratio (mean±SEM) measured on isolated mitochondria from wild-type and CIRKO mice at 24 weeks of age using PC as substrate. E, Representative blue-native PAGE (BN-PAGE). Arrows indicate separation of complexes I, II, III, IV, and V. F and G, Representative in-gel complex activity stainings and densitometric quantification (mean±SEM) of complex I, IV, and V activities of wild-type and CIRKO mice at 8 and 76 weeks of age (n=4 to 5). *$P<0.05$ vs age-matched wild-type controls.

pairment, oligomycin-treated mitochondria were maximally stimulated by exposure to the uncoupling agent FCCP. Under these conditions, oxygen consumption rates are independent of ATP synthesis and reflect maximal ETC capacity. No differences were found between 24-week-old CIRKO and control mitochondria (online-only Data Supplement Figure III). We independently determined in-gel complex I, IV, and V activities after separation of mitochondrial membrane proteins by blue-native gel electrophoresis. No differences in ETC activity were observed at any age (Figure 2E through 2G).

Mitochondrial Proteins, Gene Expression, and Mitochondrial Enzyme Activities

We also tested the hypothesis that defective mitochondrial function may result from changes in the content or activity of enzymes involved in intermediary mitochondrial metabolism that provide reducing equivalents to ETC. First, we conducted a proteomic expression analysis of mitochondrial membrane and matrix compartments (Tables 3 and 4, online-only Data Supplement Tables IIA and IIB). Ninety-three mitochondrial matrix and 151 mitochondrial membrane proteins were identified. In the mitochondrial matrix, 24 proteins were reduced in CIRKO mice relative to controls. Of these proteins, 10 were involved in FA oxidation, 10 were involved in the TCA cycle, and 3 represented subunits of pyruvate dehydrogenase (PDH) (specifically the E1 subunit and the lipoamide β subunit). In contrast, only 10 largely unrelated proteins were increased in the matrix compartment (Tables 3 and 4, online-only Data Supplement Tables IIA and IIB). In the mitochondrial membrane fraction, FA oxidation proteins also were coordinately reduced, but the pattern for oxidative phosphorylation (OXPHOS) proteins was more variable. For example, protein subunits of complex I, IV, and V were increased, whereas cytochrome C isoforms and subunits of complex III were reduced.

Second, we examined enzyme activities as a function of age, focusing on the TCA enzyme citrate synthase and the FA oxidation regulatory enzymes carnitine palmitoyl transferase-1 and 3-hydroxyacyl-CoA dehydrogenase. Relative to age-matched controls, citrate synthase activity progressively declined with age in CIRKO mice (online-only Data Supplement Figure IV). Similarly, carnitine palmitoyl transferase-1 and 3-hydroxyacyl-CoA dehydrogenase activities, which were slightly enhanced at 8 weeks, also declined with age in CIRKO mice relative to their age-matched controls (online-only Data Supplement Figure IV).

Third, we conducted a focused analysis of the expression of nuclear-encoded mitochondrial genes and confirmed

Table 3. Proteomic Analysis of Mitochondrial Membrane Proteins From CIRKO Mice

Protein	Fold Change, CIRKO/Wild Type ($P<0.05$)	Pathway
Solute carrier family 25 (mitochondrial carrier, adenine nucleotide translocator), member 13	1.16	ADP/ATP translocase
Solute carrier family 25 (mitochondrial carrier, phosphate carrier), member 3	1.08	ADP/ATP translocase
Solute carrier family 25, member 5	1.05	ADP/ATP translocase
Glutamate oxaloacetate transaminase 2, mitochondrial	0.92	Amino acid metabolism/anapleurosis/TCA
Predicted: similar to aspartate aminotransferase, mitochondrial precursor (transaminase A) (glutamate oxaloacetate transaminase 2)	0.93	Amino acid metabolism/anapleurosis
Electron transferring flavoprotein, dehydrogenase	0.86	Electron transfer to complex II
2,4-Dienoyl CoA reductase 1, mitochondrial	0.86	FA β-oxidation
Acetyl-CoA acyltransferase 2 (mitochondrial 3-oxoacyl-CoA thiolase)	0.83	FA β-oxidation
Acetyl-CoA dehydrogenase, long-chain (Mus musculus)	1.14	FA β-oxidation
Acyl-CoA synthetase long-chain family member 1	0.87	FA β-oxidation
Acyl-CoA dehydrogenase, very long chain	0.80	FA β-oxidation
Carnitine acetyltransferase	0.79	FA β-oxidation
Carnitine palmitoyltransferase 2	0.68	FA β-oxidation
Hydroxyacyl-CoA dehydrogenase/3-ketoacyl-CoA thiolase/enoyl-CoA hydratase (trifunctional protein), α subunit	0.90	FA β-oxidation
Hydroxyacyl-CoA dehydrogenase/3-ketoacyl-CoA thiolase/enoyl-CoA hydratase (trifunctional protein), β subunit	0.76	FA β-oxidation
Predicted: similar to acyl-CoA synthetase long-chain family member 1 isoform 4	0.88	FA β-oxidation
Predicted: similar to acyl-CoA synthetase long-chain family member 1 isoform 5	0.88	FA β-oxidation
Predicted: similar to hydroxyacyl-CoA dehydrogenase/3-ketoacyl-CoA thiolase/enoyl-CoA hydratase (trifunctional protein), β subunit	0.75	FA β-oxidation
Dihydrolipoamide S-acetyltransferase (E2 component of pyruvate dehydrogenase complex) (Mus musculus)	1.19	Glucose oxidation
Pyruvate dehydrogenase (lipoamide)-β	1.12	Glucose oxidation
3-Oxoacid CoA transferase 1 (Mus musculus)	1.23	Ketone metabolism
Tu translation elongation factor, mitochondrial	1.2	Mitochondrial chaperone, mitochondrial protein translation
NADH dehydrogenase (ubiquinone) 1α subcomplex, 9 (Mus musculus)	1.12	OXPHOS complex I
NADH dehydrogenase (ubiquinone) Fe-S protein 1	1.11	OXPHOS complex I
NADH dehydrogenase (ubiquinone) Fe-S protein 6	1.18	OXPHOS complex I
Predicted: similar to NADH dehydrogenase (ubiquinone) Fe-S protein 3	1.11	OXPHOS complex I
Predicted: similar to NADH dehydrogenase (ubiquinone) Fe-S protein 6	1.23	OXPHOS complex I
Cytochrome c-1	0.87	OXPHOS complex III
Ubiquinol cytochrome c reductase core protein 2	0.94	OXPHOS complex III
Cytochrome c oxidase subunit IV isoform 1 (Mus musculus)	1.09	OXPHOS complex IV
ATP synthase, H^+ transporting, mitochondrial F1 complex, α subunit, isoform 1	0.96	OXPHOS complex V
ATP synthase, H^+ transporting, mitochondrial F1 complex, δ subunit precursor (Mus musculus)	1.08	OXPHOS complex V
ATP synthase, H^+ transporting, mitochondrial F1 complex, γ subunit (Mus musculus)	1.09	OXPHOS complex V
Cytochrome c, somatic	0.87	OXPHOS cytochrome c
Predicted: similar to cytochrome c, somatic	0.87	OXPHOS cytochrome c
Predicted: similar to cytochrome c, somatic isoform 1	0.87	OXPHOS cytochrome c
PREDICTED: similar to Cytochrome c, somatic isoform 2	0.87	OXPHOS cytochrome c
Creatine kinase, mitochondrial 1, ubiquitous	0.84	Phosphotransfer
Creatine kinase, mitochondrial 2	0.76	Phosphotransfer
Nicotinamide nucleotide transhydrogenase	1.23	Proton transport and NADPH regeneration

(*Continued*)

Table 3. Continued

Protein	Fold Change, CIRKO/Wild Type ($P<0.05$)	Pathway
Citrate synthase–like protein (Mus musculus)	1.12	TCA
Dihydrolipoamide S-succinyltransferase (E2 component of 2-oxo-glutarate complex) (Mus musculus)	1.19	TCA
Isocitrate dehydrogenase 2 ($NADP^+$), mitochondrial (Mus musculus)	1.43	TCA
Malate dehydrogenase 2, NAD (mitochondrial)	0.93	TCA
Oxoglutarate dehydrogenase (lipoamide)	1.12	TCA (ROS production)
Heat shock protein 9A (Mus musculus)	1.27	Unknown
Hypothetical protein LOC237880 (Mus musculus)	1.16	Unknown

global reduction in expression of genes involved in cellular and mitochondrial FA uptake and β-oxidation and reduced expression of their transcriptional regulator peroxisome proliferator-activated receptor-α (Table 5, online-only Data Supplement Figure V). The mRNA of the *E1α1* subunit of PDH was reduced by 27%. In contrast, genes that regulate mitochondrial biogenesis were essentially unaltered, except for *SIRT1* (a potential regulator of PGC-1α activity), the expression of which was reduced by 31%. Consistent with the proteomic analysis, expression of the subunit of complex III (*Uqcrc1*) was reduced by 20% to 30% ($P<0.05$), whereas the expression of the complex I subunit (*Ndufa9*) was not statistically different from controls. Uncoupling protein expression (*UCP2* and *UCP3*) was not increased despite evidence of mitochondrial uncoupling. PDH kinase (*PDK4*) expression was reduced in 8- and 24-week-old mice, making it unlikely that reduced pyruvate flux resulted from increased phosphorylation of the E1 subunit of the PDH complex. This was confirmed by blotting for phosphorylated PDHE1, which was not altered in CIRKO hearts (online-only Data Supplement Figure VI).

Contribution of Increased Oxidative Stress to Mitochondrial Phenotypes of CIRKO Mice

To test the hypothesis that oxidative stress contributed to mitochondrial dysfunction and mitochondrial uncoupling, we measured H_2O_2 generation and the activity of mitochondrial aconitase, the activity of which is susceptible to oxidative stress.[31] Mitochondrial aconitase activity was reduced by 38% and 47% in 8- and 24-week-old CIRKO mice, respectively (Figure 3A), in the absence of proportionate differences in aconitase protein levels (data not shown). H_2O_2 production was increased by 15% and 28% in 8- and 24-week-old CIRKO mice, respectively, compared with age-matched controls (Figure 3B) after exposure to PC. Manganese superoxide dismutase and catalase protein expression was not significantly different between CIRKO and wild-type mice at 8 weeks (data not shown). These data support the hypothesis that increased mitochondrial ROS production could be an early or primary defect in CIRKO mitochondria.

To test the hypothesis that reactive oxygen species (ROS) may contribute to the increased uncoupling in 8-week-old CIRKO (as evidenced by increased V_{ADP} without an accompanying increase in ATP synthesis and increased oligomycin-insensitive respirations [V_{Oligo}]), we treated CIRKO mice with the superoxide dismutase mimetic MnTBAP for 4 weeks starting at 4 weeks of age. Treatment with MnTBAP reversed the decline in aconitase activity in both the cytosolic (data not shown) and mitochondrial fractions (Figure 3C) and prevented the increase in V_{Oligo} in cardiac fibers from 8-week-old CIRKO mice (Figure 3D). These data suggest that ROS may be partially responsible for mitochondrial uncoupling in CIRKO mouse hearts.

Insulin Signal Transduction

PI3K signaling modulates mitochondrial FA oxidative capacity.[32] Thus, we determined whether differences in PI3K signaling pathways contribute to the mitochondrial phenotypes observed. CIRKO mice exhibited a significant increase in the expression of IGF-1 receptors. Moreover, no reduction was found in basal levels of Akt and GSK3β phosphorylation, which trended higher. Whereas insulin stimulation significantly increased Akt and GSK3β phosphorylation in the control hearts, no statistical increase in either Akt or GSK3β phosphorylation after perfusion of CIRKO hearts with 1 nM insulin was observed (online-only Data Supplement Figure VII).

Mitochondrial Number and Ultrastructure Are Altered in CIRKO Mice

Mitochondrial morphology was normal in younger CIRKO mouse hearts, but at 54 weeks, mitochondria appeared dysmorphic with reduced crista density (Figure 4A). Mitochondrial number and volume density were increased at all ages examined (Figure 4B and 4C). These changes occurred despite the absence of any increase in the expression of genes involved in mitochondrial biogenesis and mitochondrial DNA replication such as peroxisome proliferator-activated receptor-γ coactivators α and β (*PGC1α*, *PGC1β*) and nuclear respiratory factors (*NRF1* or *NRF2*). Indeed, transcription factor A mitochondrial expression was reduced in 3-week-old mice (Table 5).

Discussion

Perinatal loss of insulin signaling in cardiomyocytes impairs mitochondrial function. An early defect exists in pyruvate use and a progressive reduction in mitochondrial oxidative capacity and ATP synthesis with glutamate and PC substrates. A modest decline in cardiac contractility occurs at an early

Table 4. Proteomic Analysis of Mitochondrial Matrix Proteins From CIRKO Mice

Protein	Fold Change, CIRKO/Wild Type ($P<0.05$)	Pathway
Glutamate oxaloacetate transaminase 2, mitochondrial	0.88	Amino acid metabolism/anapleurosis/TCA
Predicted: similar to aspartate aminotransferase, mitochondrial precursor (transaminase A) (glutamate oxaloacetate transaminase 2)	0.88	Amino acid metabolism/anapleurosis/TCA
Acetyl-CoA acyltransferase 2 (mitochondrial 3-oxoacyl-CoA thiolase)	0.74	FA β-oxidation
Acetyl-CoA dehydrogenase, long chain	0.89	FA β-oxidation
Acetyl-CoA dehydrogenase, medium chain	0.76	FA β-oxidation
Acyl-CoA dehydrogenase, short chain	0.71	FA β-oxidation
Acyl-CoA dehydrogenase, very long chain	1.52	FA β-oxidation
Dodecenoyl-CoAδ isomerase (3,2 trans-enoyl-CoA isomerase)	0.77	FA β-oxidation
Enoyl CoA hydratase, short chain, 1, mitochondrial	0.88	FA β-oxidation
Hydroxyacyl-CoA dehydrogenase/3-ketoacyl-CoA thiolase/enoyl-CoA hydratase (trifunctional protein), β subunit	1.37	FA β-oxidation
L-3-hydroxyacyl-CoA dehydrogenase, short chain	0.70	FA β-oxidation
Predicted: similar to hydroxyacyl-CoA dehydrogenase/3-ketoacyl-CoA thiolase/enoyl-CoA hydratase (trifunctional protein), β subunit	1.33	FA β-oxidation
Electron transferring flavoprotein, α polypeptide	0.89	FA metabolism
Electron transferring flavoprotein, β polypeptide	0.94	FA metabolism
Thioesterase superfamily member 2	0.59	FA metabolism
Predicted: similar to pyruvate dehydrogenase E1 component α subunit, somatic form, mitochondrial precursor (PDHE1-A type I) isoform 2	0.76	Glucose oxidation
Pyruvate dehydrogenase (lipoamide) β	0.86	Glucose oxidation
Pyruvate dehydrogenase E1α1	0.75	Glucose oxidation
3-Oxoacid CoA transferase 1	1.23	Ketone metabolism
Inner membrane protein, mitochondrial	1.28	(Mitofillin) required for normal mitochondrial inner membrane morphology
Predicted: similar to coiled-coil-helix-coiled-coil-helix domain containing 3 isoform 2	1.28	Mitofillin binding partner
ATP synthase, H^+ transporting mitochondrial F1 complex, β subunit	1.37	OXPHOS complex V
ATP synthase, H^+ transporting, mitochondrial F1 complex, α subunit, isoform 1	1.37	OXPHOS complex V
Aconitase 2, mitochondrial	0.92	TCA
Aldehyde dehydrogenase family 6, subfamily A1	0.83	TCA
Citrate synthase	0.9	TCA
Fumarate hydratase 1	0.92	TCA
Isocitrate dehydrogenase 2 ($NADP^+$), mitochondrial	1.06	TCA
Isocitrate dehydrogenase 3 (NAD^+) α	0.78	TCA
Oxoglutarate dehydrogenase (lipoamide)	0.77	TCA
Predicted: similar to malate dehydrogenase, mitochondrial precursor	0.87	TCA
Succinate-CoA ligase, ADP-forming, β subunit	0.61	TCA
Predicted: similar to 60-kDa heat shock protein, mitochondrial precursor (Hsp60) (60-kDa chaperonin) (CPN60) (heat shock protein 60) (HSP-60) (mitochondrial matrix protein P1) (HSP-65)	0.8	Unknown

age, which does not progress to heart failure; however, cardiac function was significantly impaired in vitro after calcium-induced inotropic stress. Two mechanisms for mitochondrial dysfunction were identified. First, a coordinate reduction was found in TCA and FA enzymes that presumably impaired the delivery of reducing equivalents to the ETC, which remained functionally competent. Second, mitochondria from insulin receptor–deficient myocytes were more susceptible to FA-induced oxidative stress and mitochondrial uncoupling. These changes promote a mitochondrial biogenic response that occurs in the absence of increased PGC-1α expression. These data identify an important role for insulin signaling pathways in modulating mitochondrial bioenergetics and integrity. We recently reported that PI3K signaling regulates mitochondrial function in the heart.[32] The present study now shows that insulin signaling

Table 5. Relative Changes in Gene Expression in CIRKO and Wild-Type Mice

	Wild Type	CIRKO, 3 Weeks	CIRKO, 8 Weeks	CIRKO, 14–24 Weeks
FA Metabolism				
ACADM (*MCAD*)	1	0.7†	0.7†	0.7*
CPT1b	1	1	0.9	0.9
CPT2	1	0.7†	0.5†	0.6†
CD36	1	0.8*	0.7*	0.7*
FABP	1	0.8†	0.7*	0.7*
PPARα	1	0.7*	0.7*	0.7
Mitochondrial biogenesis				
PGC1α	1	N/D	1.01	1.08
PGC1β	1	N/D	0.98	0.89
(*ESRRA*) *ERR*α	1	1.4	0.6	1
TFAM	1	0.7*	1	0.9
NRF1	1	1	1	0.7
NRF2	1	0.9	1	0.8
SIRT1	1	N/D	0.69*	N/D
Oxidative phosphorylation				
Ndufa9	1	0.8	0.9	0.8
Uqcrc1	1	0.7*	0.7*	0.8*
Others				
UCP2	1	0.9	0.9	0.9
UCP3	1	1.2	0.8	0.5†
PDK4	1	1.5	0.3*	0.6
PDHA1	1	N/D	0.72†	N/D
CKMT2 (*MTCK*)	1	0.7*	0.7†	0.7*
MTE1	1	0.9	0.6*	0.6*

N/D indicates not done. Full gene names are given in online-only Data Supplement Table I. Total RNA from 6 wild-type and 6 CIRKO hearts at each age was quantified by real-time polymerase chain reaction and normalized to cyclophilin expression. Values represent fold change in mRNA levels relative to wild type, which were assigned 1.

*$P<0.05$, †$P<0.005$ versus age-matched wild-type controls.

per se also regulates myocardial mitochondrial oxygen consumption and ATP synthesis rates. The blunted activation of PI3K targets such as Akt and its downstream substrate GSK3β in insulin-perfused CIRKO hearts is consistent with the hypothesis that reduced PI3K signaling could contribute to mitochondrial dysfunction in CIRKO hearts. However, given that basal levels of phosphorylation of these kinases were not reduced, it is also likely that PI3K- or Akt-independent signals downstream of the insulin receptor also play an important role.

The mitochondrial defect appears initially to be specific for pyruvate use and subsequently for FA use. These observations provide a mechanistic basis for our previously published observations that in isolated perfused working hearts from 16- to 20- week-old CIRKO mice, rates of both glucose and FA oxidation were reduced.[23] An important mechanism for reduced pyruvate flux appears to be reduced content of 2 key subunits of the PDH complex. The E1α subunit is a key regulator of PDH flux and is the substrate of the regulatory kinase PDK4.[33,34] We provide novel evidence that the E1α1 subunit of PDH may be an insulin-regulated transcript in the heart and that reduced protein levels of this subunit in mitochondrial matrix might occur on the basis of transcriptional repression. Increased phosphorylation of the E1α subunit by PDK4 decreases its stability, whereas blocking degradation of the E1α subunit of PDH increases the activity of and flux through the enzyme complex.[35] However, PDHE1 phosphorylation was not increased in CIRKO hearts, and the expression of its kinase (PDK4) was actually reduced. Mitochondrial dysfunction in CIRKO mice is associated with a modest reduction in cardiac function. We previously reported that cardiac function was reduced in isolated working hearts that were perfused with glucose and FA as substrates under normal workload.[23] In the present study, we chose to study glucose-perfused hearts because of the defect in pyruvate use in mitochondria. We reasoned that in the presence of glucose alone, contractile dysfunction after calcium-induced inotropic stress would be amplified.

We speculate that an early defect in glucose/pyruvate metabolism could initially lead to the increase in FA use that was observed in the mitochondria of 8-week-old CIRKO mice. However, this cannot be sustained over time because of the coordinate reduction in levels of mitochondrial β-oxidation enzymes. This hypothesis also is supported by the observation of increased rates of FA oxidation in isolated working hearts obtained from 8-week-old CIRKO mice (see online-only Data Supplement Figure VIII) but reduced FA oxidation in 16- to 20-week-old mice.[23] The reduction in gene and protein expression levels of a broad array of regulators of FA metabolism was striking and extends our previously reported findings that demonstrated reduced mRNA for acyl CoA dehydrogenases. The likely mechanism for these changes is insulin-mediated regulation of expression levels of the peroxisome proliferator-activated receptor-α gene in the heart.

The second major mechanism that contributed to mitochondrial dysfunction is oxidative stress and ROS-mediated mitochondrial dysfunction. Increased ROS production was evident in the hearts of 8-week-old CIRKO mice and was sufficient to reduce the activity levels of the redox-sensitive enzyme aconitase. This increase in ROS also likely reduced mitochondrial energetics by promoting mitochondrial uncoupling as evidenced by reduced ATP/O ratios in PC-treated mitochondria and increased oligomycin-insensitive respiration rates that were normalized by treating animals with the antioxidant MnTBAP. MnTBAP reduces ROS but could increase H_2O_2 generation, underscoring that mitochondrial superoxide likely mediates the changes observed. Increased ROS could reflect changes in superoxide generation or detoxification. Although increased FA flux could contribute to increased ROS production in 8-week-old CIRKO hearts, it is unlikely to represent the mechanism in older hearts in which FA oxidation is reduced. Proteomic analysis revealed changes in stoichiometry of ETC subunits, which could potentially contribute to increased superoxide generation. A major role for a reduction in ROS degradation pathways as a contributor to increased H_2O_2 production in CIRKO mitochondria appears unlikely because neither manganese superoxide dismutase levels nor catalase content was changed in 8-week-old mice and catalase content was marginally lower

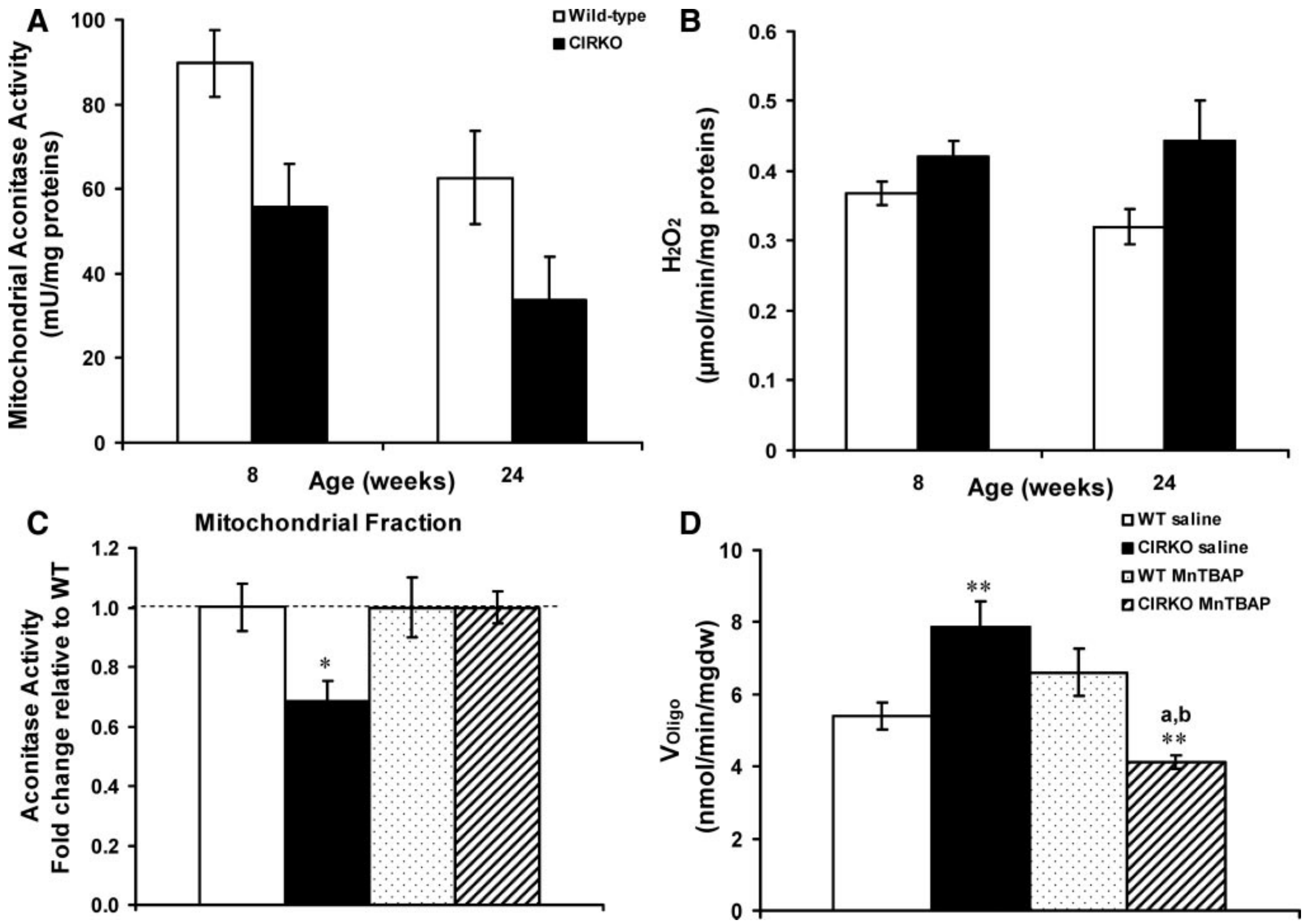

Figure 3. Increased oxidative stress in CIRKO hearts. Data are mean±SEM. A, Aconitase activity measured in mitochondria isolated from 8- and 24-week-old CIRKO (black bars; n=5) and wild-type (white bars; n=6) hearts. Statistics (2-way ANOVA): WT vs CIRKO, $P<0.05$ and $P<0.005$ at 8 and 24 weeks, respectively. B, H_2O_2 production in isolated mitochondria obtained from 8- and 24-week-old CIRKO (n=7) and wild-type (n=7). Mitochondria were incubated with PC and L-carnitine in the presence of oligomycin as described in Methods. Statistics (2-way ANOVA): WT vs CIRKO, $P<0.005$. C, Mitochondrial aconitase activity determined in saline-treated wild-type (open bars; n=6 per group) and CIRKO (black bars, n=6) mice and MnTBAP-treated wild-type (dotted bars; n=6) and CIRKO (hatched bars; n=6) mice at 8 weeks of age. D, Oligomycin-insensitive respiration ($V_{oligomycin}$) in saponin-permeabilized cardiac fibers from wild-type (saline and MnTBAP) and CIRKO (saline and MnTBAP) mice at 8 weeks of age. *$P<0.05$, **$P<0.005$ vs wild type; $^aP<0.005$ vs CIRKO saline; $^bP<0.005$ vs wild-type MnTBAP (1-way ANOVA).

in 24-week-old mice. However, it is possible that reduced TCA flux could limit the supply of reducing equivalents to replenish NADPH pools that maintain antioxidants such as glutathione in the reduced state. Taken together, deficient insulin signaling in the heart likely promotes mitochondrial oxidative stress by multiple mechanisms.

Mitochondrial biogenesis has been described in the hearts of insulin-resistant mice and has been attributed to activation of PGC-1α–mediated signaling.[36] Here, we show that mitochondrial number and volume density increased in CIRKO mice despite the lack of coordinate changes in mRNA levels of key regulators of the mitochondrial biogenesis pathway such as PGC-1α. Thus, the possibility exists that this proliferative response in CIRKO hearts is a consequence of reduced ATP generation or increased oxidative stress, which promote mitochondrial biogenesis. In this regard, it is important to discuss the discrepancy between citrate synthase activities and increased mitochondrial volume density in aging CIRKO mice. Citrate synthase activity is widely used as an indirect estimate of mitochondrial mass. However, in CIRKO mice, our proteomic analyses indicate that citrate synthase protein content in mitochondrial matrix was already significantly lower in 8-week-old CIRKO mice. This observation therefore supports the notion that the morphological "biogenic" response that we observed represents an adaptation to preexisting mitochondrial dysfunction in this model.

Conclusions

We demonstrate that insulin signaling is a regulator of mitochondrial oxidative capacity via mechanisms that may determine TCA cycle flux and the mitochondrial metabolism of pyruvate and FAs. Moreover, impaired insulin signaling predisposes cardiac mitochondria to oxidative stress, which not only might damage mitochondria but also impairs energetics by activating mitochondrial uncoupling. Thus, insulin signaling plays an essential role in the maintenance of mitochondrial homeostasis in the heart. Given the perinatal timing of insulin receptor deletion in CIRKO hearts, it is important to note that metabolic maturation of the heart continues to occur throughout the neonatal period; thus, we

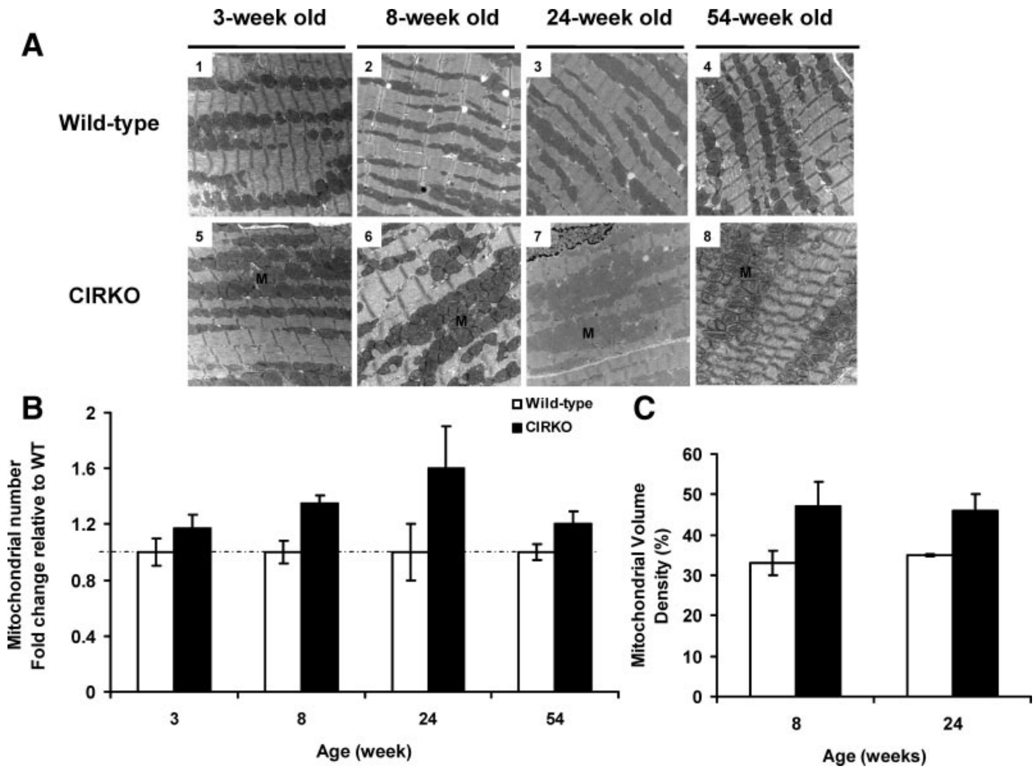

Figure 4. Mitochondrial number and morphology in CIRKO and wild-type hearts. A, Representative electron micrographs of heart sections (80 to 100 nm) from 3-, 8-, 24-, and 54-week-old wild-type (1 through 4) and CIRKO (5 through 8) mice (3 per group). B, Quantification of mitochondrial number in CIRKO hearts (fold change vs wild-type normalized to 1±SEM). Statistics (2-way ANOVA): WT vs CIRKO, $P<0.005$. C, Mitochondrial volume density relative to cell area in wild-type and CIRKO mice at 8 and 24 weeks of age. Statistics (2-way ANOVA): WT vs CIRKO, $P<0.005$.

cannot rule out that the phenotypes that we have observed might reflect unique effects of insulin resistance during this important developmental window. Future studies in mice with inducible knockout of insulin receptors in adult hearts are required for clarification.

Diabetes mellitus and obesity are independent risk factors for the development of heart failure.[37] A growing body of evidence indicates that acquired defects in insulin signaling, which may impair cardiac metabolism and are associated with left ventricular dysfunction, develop in the heart in diabetes mellitus and obesity.[38] The present study provides new insights into potential mechanisms linking impaired postnatal insulin signaling with the development of mitochondrial dysfunction in the heart.

Acknowledgment

We thank James Metherall, PhD, for use of robotic facilities for gene expression analysis.

Sources of Funding

This work was supported by grants RO1HL070070, R21DK073590 (funded by the office of Dietary Supplements and the NIDDK), UO1HL70525, and UO1HL087947 from the National Institutes of Health and 19–2006–1071 from the Juvenile Diabetes Research Foundation to Dr Abel, who is an Established Investigator of the American Heart Association, and by a grant from the Department of Veterans Affairs to Dr Litwin. Dr Boudina was supported by postdoctoral fellowships from the Juvenile Diabetes Research Foundation and the American Heart Association. Dr Bugger was supported by a postdoctoral fellowship of the German Research Foundation. Dr Zaha is supported by a postdoctoral fellowship from the AHA; Dr O'Neill, by a physician scientist-training award from the American Diabetes Association; and Dr Palfreyman, by a summer research grant from the Endocrine Society.

Disclosures

None.

References

1. Boudina S, Abel ED. Mitochondrial uncoupling: a key contributor to reduced cardiac efficiency in diabetes. *Physiology (Bethesda)*. 2006;21:250–258.
2. Boudina S, Abel ED. Diabetic cardiomyopathy revisited. *Circulation*. 2007;115:3213–3223.
3. Boudina S, Sena S, O'Neill BT, Tathireddy P, Young ME, Abel ED. Reduced mitochondrial oxidative capacity and increased mitochondrial uncoupling impair myocardial energetics in obesity. *Circulation*. 2005; 112:2686–2695.
4. Boudina S, Sena S, Theobald H, Sheng X, Wright JJ, Hu XX, Aziz S, Johnson JI, Bugger H, Zaha VG, Abel ED. Mitochondrial energetics in the heart in obesity-related diabetes: direct evidence for increased uncoupled respiration and activation of uncoupling proteins. *Diabetes*. 2007;56:2457–2466.
5. Bugger H, Boudina S, Hu XX, Tuinei J, Zaha VG, Theobald HA, Yun UJ, McQueen AP, Wayment B, Litwin SE, Abel ED. Type 1 diabetic Akita mouse hearts are insulin sensitive but manifest structurally abnormal mitochondria that remain coupled despite increased uncoupling protein 3. *Diabetes*. 2008;57:2924–2932.
6. Peterson LR, Herrero P, Schechtman KB, Racette SB, Waggoner AD, Kisrieva-Ware Z, Dence C, Klein S, Marsala J, Meyer T, Gropler RJ. Effect of obesity and insulin resistance on myocardial substrate metabolism and efficiency in young women. *Circulation*. 2004;109:2191–2196.
7. Scheuermann-Freestone M, Madsen PL, Manners D, Blamire AM, Buckingham RE, Styles P, Radda GK, Neubauer S, Clarke K. Abnormal cardiac and skeletal muscle energy metabolism in patients with type 2 diabetes. *Circulation*. 2003;107:3040–3046.

8. Liang Q, Carlson EC, Donthi RV, Kralik PM, Shen X, Epstein PN. Overexpression of metallothionein reduces diabetic cardiomyopathy. *Diabetes*. 2002;51:174–181.
9. Shen X, Zheng S, Metreveli NS, Epstein PN. Protection of cardiac mitochondria by overexpression of MnSOD reduces diabetic cardiomyopathy. *Diabetes*. 2006;55:798–805.
10. Shen X, Zheng S, Thongboonkerd V, Xu M, Pierce WM Jr, Klein JB, Epstein PN. Cardiac mitochondrial damage and biogenesis in a chronic model of type 1 diabetes. *Am J Physiol Endocrinol Metab*. 2004;287:E896–E905.
11. Ye G, Metreveli NS, Ren J, Epstein PN. Metallothionein prevents diabetes-induced deficits in cardiomyocytes by inhibiting reactive oxygen species production. *Diabetes*. 2003;52:777–783.
12. Desrois M, Sidell RJ, Gauguier D, King LM, Radda GK, Clarke K. Initial steps of insulin signaling and glucose transport are defective in the type 2 diabetic rat heart. *Cardiovasc Res*. 2004;61:288–296.
13. Mazumder PK, O'Neill BT, Roberts MW, Buchanan J, Yun UJ, Cooksey RC, Boudina S, Abel ED. Impaired cardiac efficiency and increased fatty acid oxidation in insulin-resistant ob/ob mouse hearts. *Diabetes*. 2004;53:2366–2374.
14. Ouwens DM, Boer C, Fodor M, de Galan P, Heine RJ, Maassen JA, Diamant M. Cardiac dysfunction induced by high-fat diet is associated with altered myocardial insulin signalling in rats. *Diabetologia*. 2005;48:1229–1237.
15. Ouwens DM, Diamant M, Fodor M, Habets DD, Pelsers MM, El Hasnaoui M, Dang ZC, van den Brom CE, Vlasblom R, Rietdijk A, Boer C, Coort SL, Glatz JF, Luiken JJ. Cardiac contractile dysfunction in insulin-resistant rats fed a high-fat diet is associated with elevated CD36-mediated fatty acid uptake and esterification. *Diabetologia*. 2007;50:1938–1948.
16. Park SY, Cho YR, Kim HJ, Higashimori T, Danton C, Lee MK, Dey A, Rothermel B, Kim YB, Kalinowski A, Russell KS, Kim JK. Unraveling the temporal pattern of diet-induced insulin resistance in individual organs and cardiac dysfunction in C57BL/6 mice. *Diabetes*. 2005;54:3530–3540.
17. Abel ED. Glucose transport in the heart. *Front Biosci*. 2004;9:201–215.
18. Brownsey RW, Boone AN, Allard MF. Actions of insulin on the mammalian heart: metabolism, pathology and biochemical mechanisms. *Cardiovasc Res*. 1997;34:3–24.
19. Slot JW, Geuze HJ, Gigengack S, James DE, Lienhard GE. Translocation of the glucose transporter GLUT4 in cardiac myocytes of the rat. *Proc Natl Acad Sci U S A*. 1991;88:7815–7819.
20. Watanabe T, Smith MM, Robinson FW, Kono T. Insulin action on glucose transport in cardiac muscle. *J Biol Chem*. 1984;259:13117–13122.
21. Lawson JW, Uyeda K. Effects of insulin and work on fructose 2,6-bisphosphate content and phosphofructokinase activity in perfused rat hearts. *J Biol Chem*. 1987;262:3165–3173.
22. Stavinoha MA, RaySpellicy JW, Essop MF, Graveleau C, Abel ED, Hart-Sailors ML, Mersmann HJ, Bray MS, Young ME. Evidence for mitochondrial thioesterase 1 as a peroxisome proliferator-activated receptor-alpha-regulated gene in cardiac and skeletal muscle. *Am J Physiol Endocrinol Metab*. 2004;287:E888–E895.
23. Belke DD, Betuing S, Tuttle MJ, Graveleau C, Young ME, Pham M, Zhang D, Cooksey RC, McClain DA, Litwin SE, Taegtmeyer H, Severson D, Kahn CR, Abel ED. Insulin signaling coordinately regulates cardiac size, metabolism, and contractile protein isoform expression. *J Clin Invest*. 2002;109:629–639.
24. Hu P, Zhang D, Swenson L, Chakrabarti G, Abel ED, Litwin SE. Minimally invasive aortic banding in mice: effects of altered cardiomyocyte insulin signaling during pressure overload. *Am J Physiol*. 2003;285:H1261–H1269.
25. Sena S, Rasmussen IR, Wende AR, McQueen AP, Theobald HA, Wilde N, Pereira RO, Litwin SE, Berger JP, Abel ED. Cardiac hypertrophy caused by peroxisome proliferator-activated receptor-gamma agonist treatment occurs independently of changes in myocardial insulin signaling. *Endocrinology*. 2007;148:6047–6053.
26. Veksler VI, Kuznetsov AV, Sharov VG, Kapelko VI, Saks VA. Mitochondrial respiratory parameters in cardiac tissue: a novel method of assessment by using saponin-skinned fibers. *Biochim Biophys Acta*. 1987;892:191–196.
27. Rolfe DF, Hulbert AJ, Brand MD. Characteristics of mitochondrial proton leak and control of oxidative phosphorylation in the major oxygen-consuming tissues of the rat. *Biochim Biophys Acta*. 1994;1188:405–416.
28. Wittig I, Braun HP, Schagger H. Blue native PAGE. *Nat Protoc*. 2006;1:418–428.
29. Weibel ER. Stereological principles for morphometry in electron microscopic cytology. *Int Rev Cytol*. 1969;26:235–302.
30. Silva JC, Denny R, Dorschel CA, Gorenstein M, Kass IJ, Li GZ, McKenna T, Nold MJ, Richardson K, Young P, Geromanos S. Quantitative proteomic analysis by accurate mass retention time pairs. *Anal Chem*. 2005;77:2187–2200.
31. Fillebeen C, Pantopoulos K. Redox control of iron regulatory proteins. *Redox Rep*. 2002;7:15–22.
32. O'Neill BT, Kim J, Wende AR, Theobald HA, Tuinei J, Buchanan J, Guo A, Zaha VG, Davis DK, Schell JC, Boudina S, Wayment B, Litwin SE, Shioi T, Izumo S, Birnbaum MJ, Abel ED. A conserved role for phosphatidylinositol 3-kinase but not Akt signaling in mitochondrial adaptations that accompany physiological cardiac hypertrophy. *Cell Metab*. 2007;6:294–306.
33. Harris RA, Bowker-Kinley MM, Huang B, Wu P. Regulation of the activity of the pyruvate dehydrogenase complex. *Adv Enzyme Regul*. 2002;42:249–259.
34. Sugden MC, Holness MJ. Recent advances in mechanisms regulating glucose oxidation at the level of the pyruvate dehydrogenase complex by PDKs. *Am J Physiol Endocrinol Metab*. 2003;284:E855–E862.
35. Morten KJ, Caky M, Matthews PM. Stabilization of the pyruvate dehydrogenase E1alpha subunit by dichloroacetate. *Neurology*. 1998;51:1331–1335.
36. Duncan JG, Fong JL, Medeiros DM, Finck BN, Kelly DP. Insulin-resistant heart exhibits a mitochondrial biogenic response driven by the peroxisome proliferator-activated receptor-alpha/PGC-1alpha gene regulatory pathway. *Circulation*. 2007;115:909–917.
37. Abel ED. Myocardial insulin resistance and cardiac complications of diabetes. *Curr Drug Targets Immune Endocr Metabol Disord*. 2005;5:219–226.
38. Abel ED, Litwin SE, Sweeney G. Cardiac remodeling in obesity. *Physiol Rev*. 2008;88:389–419.

CLINICAL PERSPECTIVE

Obesity and diabetes mellitus may increase the risk of heart failure. The mechanisms are multifactorial, but recent studies have implicated a potential role for mitochondrial dysfunction. Studies in animal models of obesity and type 2 diabetes mellitus have suggested that insulin resistance develops in the myocardium. However, the consequences of insulin resistance in the heart are incompletely understood. The present study sought to determine whether impaired myocardial insulin signaling could impair mitochondrial function in the heart. Using genetically engineered mice with deletion of insulin receptors in cardiomyocytes, we show that impaired myocardial insulin signaling leads to multiple mitochondrial defects that include reduced oxygen consumption and ATP synthesis, reduced levels of mitochondrial enzymes that regulate pyruvate and fatty acid metabolism, and decreased content of citric acid cycle (tricarboxylic acid) proteins. Insulin signaling also regulates the expression of genes such as peroxisome proliferator-activated receptor-α in the heart, which controls the capacity of mitochondria to oxidize fatty acids. In addition, mitochondria from hearts with defective insulin signaling demonstrate evidence of oxidative stress. This study identifies novel roles for insulin signal transduction in the regulation of cardiac mitochondrial function and identifies mechanisms that could potentially contribute to myocardial dysfunction when the heart becomes insulin resistant.

Circulation

Contribution of Impaired Myocardial Insulin Signaling to Mitochondrial Dysfunction and Oxidative Stress in the Heart

Sihem Boudina, Heiko Bugger, Sandra Sena, Brian T. O'Neill, Vlad G. Zaha, Olesya Ilkun, Jordan J. Wright, Pradip K. Mazumder, Eric Palfreyman, Timothy J. Tidwell, Heather Theobald, Oleh Khalimonchuk, Benjamin Wayment, Xiaoming Sheng, Kenneth J. Rodnick, Ryan Centini, Dong Chen, Sheldon E. Litwin, Bart E. Weimer and E. Dale Abel

Circulation. 2009;119:1272-1283; originally published online February 23, 2009;
doi: 10.1161/CIRCULATIONAHA.108.792101
Circulation is published by the American Heart Association, 7272 Greenville Avenue, Dallas, TX 75231

Print ISSN: 0009-7322. Online ISSN: 1524-4539

SUPPLEMENTAL MATERIAL

CONTRIBUTION OF IMPAIRED MYOCARDIAL INSULIN SIGNALING TO MITOCHONDRIAL DYSFUNCTION AND OXIDATIVE STRESS IN THE HEART

Sihem Boudina, Ph.D.[1], Heiko Bugger M.D.[1], Sandra Sena, Ph.D.[1], Brian T. O'Neill, MD. Ph.D.[1], Vlad G. Zaha, MD Ph.D.[1], Olesya Ilkun, MS.[1], Jordan J. Wright, BS.[1], Pradip K. Mazumder, DVM Ph.D.[1], Eric Palfreyman, MD.[1], Timothy J. Tidwell[1], Heather Theobald, BS.[1], Oleh Khalimonchuk, Ph.D.[2], Benjamin Wayment, BS[3], Xiaoming Sheng Ph.D.[4], Kenneth J. Rodnick, Ph.D.[5], Ryan Centini BS[6], Dong Chen Ph.D[6], Sheldon E. Litwin, MD.[3], Bart E. Weimer Ph.D.[6], E. Dale Abel, MB.BS., D.Phil.[1, 2]

SUPPLEMENTAL METHODS

Composition of animal chow

Animals were fed standard mouse chow Harland Teklad Diet 8656 that contained 24.5% protein (Soy based), 65% Carbohydrate (Corn and soybean meal), 4.4% fat (Soybean oil), 3.4% fiber and supplemented with vitamins and minerals. This diet provided 3.8 Kcal/g of gross energy.

Mitochondrial Isolation and Determination of Oxygen Consumption

Hearts were diced in STE medium [250 mmol/l sucrose, 5 mmol/l Tris/HCl (pH 7.4) and 2 mmol/l EGTA], digested on ice for 4 min in STE medium [to which was added 0.5% (w/v) BSA, 5 mmol/l $MgCl_2$, 1 mmol/l ATP and 2.5 units/ml protease (type VIII from *Bacillus licheniformis*)] and homogenized three times in a Polytron homogenizer for 3 seconds. The homogenate was then centrifuged at 8,000X g for 10 min at 4 °C. The pellets were re-suspended in STE buffer and centrifuged at 700g for 10 min at 4 °C. Finally, the supernatant is centrifuged at 8,000X g for 10 min at 4 °C to pellet the mitochondria. The protein concentration of mitochondrial suspensions was determined using a Micro BCA reagent (Pierce) with BSA as a standard. Respirations on isolated mitochondria (0.4 mg/ml) were measured at 25 °C in respiration buffer [120 mmol/l KCl, 5 mmol/l KH_2PO_4, 1 mmol/l EGTA, 3 mmol/l HEPES, 1 mg/ml BSA with either 20 μmol/l palmitoyl-carnitine with 2 mmol/l malate, or with 10 mmol/l pyruvate and 5 mmol/l malate, pH 7.2].

Blue Native Gel Electrophoresis

Mitochondrial membranes (75 µg) were solubilized using 1% dodecylmaltoside final concentration, incubated for 20 min on ice and centrifuged (20,000X g, 10 min, 4°C). Supernatants were mixed with sample buffer (5% Coomassie brilliant blue G250, 0.5 mole 6-aminocaproic acid, pH 7.0) and loaded on a 6–13% gradient polyacrylamide gel. After electrophoresis, gels were rinsed briefly with water, and horizontal gel strips were cut containing complex I, complex IV, or complex V. Gel strips were equilibrated in respective staining solution without staining reagents for 10 min, and then incubated in 10ml staining solution as described before [1]. In brief, Complex I solution contained 0.1 mg/mL NADH, 2 mmol/l Tris/HCl, and 2.5 mg/mL Nitro Blue tetrazolium chloride, pH 7.4. Complex IV solution contained 50 mmol/l phosphate buffer pH 7.4, 1 mg/ml 3,3'-diaminobenzidine, 10 µL catalase (20 mg/mL), 1 mg/ml cytochrome *c*, and 220 mmol/l sucrose. Complex V solution contained 34 mmol/l Tris, 270 mmol/l glycine, 14 mmol/l

$MgSO_4$, 0.2% lead acetate, and 8 mmol/l ATP, pH 7.8. Gel strips were incubated at room temperature (complex I) or 30°C (complex IV and V) for 10 min. Gels were then destained and fixed in 45% (v/v) methanol and 10% (v/v) acetic acid. Signal intensity was quantified using Image J software.

Mitochondrial Proteomic Analysis

Protein in-solution Tryptic Digestion: 5µl of 0.2% RapidGest (Waters, Manchester, UK) was added to 20µg of membrane protein sample in 15µl H_2O. The mixed solution was heated at 80°C for 20 minutes. The protein mixtures were then tryptically digested according to a modified digestion method in the Waters Protein Expression System Manual (Waters, 2006). After adding NH_4HCO_3 and treating with dithiothreitol (DTT) and iodoacetamide (IAA), 4 µl of 0.11 µg/µl Trypsin in 25 mM NH_4HCO_3 was added to the protein sample. The sample was then incubated at 37°C overnight and then with 1% Formic Acid for 30 minutes at 37°C, and then centrifuged at 10,000 RPM for 10 minutes. The supernatant is then analyzed by LC-MS/MS.

Expression Analysis by Mass Spectrometry: Digested protein samples (3 µl each) were introduced into a Symmetry® C18 trapping column (180 µM x 20 mm) by NanoACQUITY Sample Manager (Waters, Manchester, UK) and washed by H_2O for 2 minutes at 10 ml/min. The peptides were then eluted from the Trapping column over a 100 µm x100 mm BEH 130 C18 column with a 140 min gradient (1-4% B for 0.1 min, 4-25% B for 89.9 min, 25-35% B for 5 min, 35-85% B for 2 min, 85% B for 13 min, 85-95% B for 8 min, 95-1% B for 2 min and 1% B for 20 min) at 0.8µL/min flow rate using an

NanoACQUITY UPLC (Waters, Manchester, UK). For this system, solvent A is composed of 99.9% H_2O, 0.1% formic acid. Solvent B is composed of 99.9% acetonitrile and 0.1% formic acid. The mass spectrometry (MS) was set to a parallel fragmentation mode (MSE) with the scan times of 1.0 second. The low fragmentation energy was 5 volts and the high fragmentation ranged from 17 to 45 volts. (GLU1)-Fibrinopeptide B is used as an external calibration standard with LockSpray. Enolase is used as the spiked control. Waters ProteinLynx Global SERVER Version 2.3 was used to analyze the ms dataset.

LC/MS/MS data statistical analysis: The algorithms and statistical method used in the Waters Protein Expression System are published [2]. The key algorithm in Waters Protein Expression System is the clustering algorithm which chemically clusters peptide components by mass and retention time for all injected samples and performs binary comparisons for each of the experimental condition to generate an average normalized intensity ratio for all matched AMRT (Accurate Mass, Retention Time) components. A statistical Student's *t*-test method was used for each binary comparison.

Insulin signaling: Total proteins were extracted from whole hearts of 8 week-old mice that were perfused in the working mode with Henseleit buffer containing (in millimoles) 118.5 NaCl, 25 $NaHCO_3$, 4.7 KCl, 1.2 $MgSO_4$, 1.2 KH_2PO_4, 2.5 $CaCl_2$, 0.5 EDTA, and 5 glucose, gassed with 95% O_2-5% CO_2 and supplemented with 0.4 mM palmitate bound to 3% BSA in the presence or absence of 1 nM insulin. Hearts were frozen in liquid nitrogen and homogenized with a Polytron in Lysis Buffer (Hepes, 50 mM, pH7.5; NaCl, 150 mM; glycerol, 10%; sodium pyrophosphate, 10 mM; sodium fluoride, 100 mM;

EGTA, 1 mM; Triton X-100, 1%; protease and phosphatase inhibitor cocktail from Roche and Sigma, respectively). Samples were then incubated for 1 hour on ice and then centrifuged for 10 minutes at 14,000 g in a micro-centrifuge at 4°C. The supernatant was collected, aliquoted and stored at -80°C until use. Protein concentration was measured using Micro BCA reagent (Pierce).

Western blot analysis.

For insulin signaling, protein extracts were resolved by SDS-PAGE and electrotransferred onto PVDF membranes (Millipore Corp., Billerica, MA). Membranes were probed with the appropriate primary antibody at a dilution of 1/1000. The following antibodies were used: phospho-Akt-Ser 473 (Cell Signaling Danvers, MA), total Akt1/2 (Cell Signaling), IGF1R (Santa Cruz, Santa Cruz, CA), phospho-GSK3β-Ser9 (Cell Signaling), total GSK3β (Santa Cruz). Other antibodies used were: rabbit anti-catalase antibody (Novus Biologicals, Littleton, CO), mouse anti-MnSOD antibody (BD Biosciences, San Jose, CA), a mouse polyclonal antibody against aconitase (kind gift of Dr. Elizabeth Leibold, University of Utah), mouse anti- Cytochrome Oxidase (Complex IV) Subunit 4 (Molecular Probes, Eugene, OR) and Mfn2 (Sigma, Saint Louis, MO). To control for loading, mouse anti-α tubulin antibody (Sigma, Saint Louis, MO) was used. Protein detection was carried out with the appropriate horseradish peroxidase-conjugated secondary antibody and ECL or ECL Plus detection systems (Amersham Biosciences, Piscataway, NJ). Blots were scanned and analyzed by computerized laser densitometry using the Image J software and results were normalized against respective loading control. For pyruvate dehydrogenase E1α (PDHE1α) bots: Mouse polyclonal to PDHE1α subunit (Abcam Inc. Cambridge, MA) and the anti-Pyruvate Dehydogenase pSer^{293} Rabbit pAb (Calbiochem, San Diego, CA) were used. Alexa fluor anti-Rabbit 680 (Invitrogen, Carlsbad, CA) and Mouse 800 (VWR International, West Chester, PA) were used as secondary antibodies and fluorescence quantified using the LI-COR Odyssey imager (Lincoln, NE).

Mitochondrial enzyme activities

Total carnitine palmitoyl-transferase (CPT) (CPT 1 and CPT 2) activity was measured in isolated mitochondria from freshly excised non-perfused hearts as previously described [3]. Citrate synthase (CS) and 3-hydroxyacyl-CoA dehydrogenase (HADH) enzyme activities were assessed in frozen heart tissue (~10 mg) as previously described [3]. Aconitase activity was measured in mitochondrial fractions as described before [4].

SUPPLEMENTAL TABLES

Supplemental Table S1. Primer sequences of mouse genes used for quantification of mRNA levels by real-time PCR.

Gene Name	Sequence of forward and reverse primers (5'-3')	GeneBank reference
Medium chain acetyl-Coenzyme A dehydrogenase (ACADM)	ACTGACGCCGTTCAGATTTT GCTTAGTTACACGAGGGTGATG	NM_007382
Carnitine palmitoyltransferase 1b – muscle (CPT1B)	TGCCTTTACATCGTCTCCAA AGACCCCGTAGCCATCATC	NM_009948
Carnitine palmitoyltransferase 2 (CPT2)	CCAGCTGACCAAAGAAGCA GCAGCCTATCCAGTCATCGT	NM_009949
Pyruvate dehydrogenase kinase - isoenzyme 4 (PDK4)	GCTTGCCAATTTCTCGTCTC CTTCTCCTTCGCCAGGTTCT	NM_013743
Peroxisome proliferator activated receptor alpha (PPARA)	GAGAATCCACGAAGCCTACC AATCGGACCTCTGCCTCTTT	NM_011144
Peroxisome proliferator activated receptor gamma co-activator 1 alpha (PGC1A)	GTAAATCTGCGGGATGATGG AGCAGGGTCAAAATCGTCTG	NM_008904
Peroxisome proliferator activated receptor gamma co-activator 1 beta (PGC1B)	TGAGGTGTTCGGTGAGATTG CCATAGCTCAGGTGGAAGGA	NM_133249
Estrogen related receptor alpha (ESRRA)	GGAGGACGGCAGAAGTACAA CAGGTTCAACAACCAGCAGA	NM_007953
Transcription factor A – mitochondrial (TFAM)	CAAAAAGACCTCGTTCAGCA CTTCAGCCATCTGCTCTTCC	NM_009360
Nuclear respiratory factor 1 (NRF1)	CTTCAGAACTGCCAACCACA GCTTCTGCCAGTGATGCTAC	NM_010938
Nuclear respiratory factor 2 (NFR2)	AGTCTTCACTGCCCCTCATC TCTGTCAGTGTGGCTTCTGG	NM_010902

Uncoupling protein 2 (UCP2)	TCTCCTGAAAGCCAACCTCA CTACGTTCCAGGATCCCAAG	NM_011671
Uncoupling protein 3 (UCP3)	TGCTGAGATGGTGACCTACGA CCAAAGGCAGAGACAAAGTGA	NM_009464
Fatty acid translocase (CD36)	TCCTTGTAGGAGATGGTGTTCC CCATTGGTGATGAAAAAGCA	NM_007643
Fatty acid binding protein 3 - muscle and heart (FABP)	GACGGGAAACTCATCCTGAC TCTCCAGAAAAATCCCAACC	NM_010174
Mitochondrial creatine kinase 2 (CKMT2)	AGAACTGCGGCTCCAAAAG CACTTCCTGCCAAACTGAGG	AK009042
Mitochondrial acyl-CoA thioesterase 1 (MTE1)	GACCTCCCCAAGAGCATAGA TCCTTGTAGGAGATGGTGTTCC	NM_134188
NADH dehydrogenase (ubiquinone) 1 alpha subcomplex 9 (Ndufa9)	ATCCCTTACCCTTTGCCACT CCGTAGCACCTCAATGGACT	NM_025358
Ubiquinol-cytochrome c reductase core protein 1 (Uqcrc1)	TGCCAGAGTTTCCAGACCTT CCAAATGAGACACCAAAGCA	NM_025407
Cyclophilin A (CPHN)	AGCACTGGAGAGAAAGGATTTG G TCTTCTTGCTGGTCTTGCCATT	NM_008907
Pyruvate dehydrogenase E1α1 (PDHA1)	GGGACGTCTGTTGAGAGAGC TGTGTCCATGGTAGCGGTAA	NM_008810

Primer pairs were designed based on GenBank reference sequences. We used the WWW interface Primer 3 (http://frodo.wi.mit.edu/cgi_bin/primer3/primer3_www.cgi) with default settings. To avoid non specific amplifications, primer sequences were blasted against mouse genes. Dissociation curves were analyzed for all primer-pairs to ensure single product amplification.

Supplemental Table S2A. Proteomic Analysis of all Mitochondrial Membrane Proteins from CIRKO Mice.

Accession	OK	Description	Score	Unique	Matrix-WT-20070913:Matrix-TG-20070913_Ratio	Matrix-WT-20070913:Matrix-TG-20070913_Log(e) Ratio	Matrix-WT-20070913:Matrix-TG-20070913_Log(e) StdDev	Matrix-WT-20070913:Matrix-TG-20070913__P	Matrix-TG-20070913_Rel Profile	Matrix-TG-20070913_Rel Profile SD	Matrix-WT-20070913_Rel Profile	Matrix-WT-20070913_Rel Profile SD
NP_080448.1	2	2,4-dienoyl CoA reductase 1, mitochondrial [Mus musculus]	358.88		1.16	0.15	0.12	0.99	0.92	0.06	1.08	0.06
NP_077150.1	2	3-oxoacid CoA transferase 1 [Mus musculus]	371.67		0.81	-0.21	0.19	0.01	1.11	0.09	0.89	0.09
NP_659033.1	2	acetyl-Coenzyme A acetyltransferase 1 precursor [Mus musculus]	648.11		1.05	0.05	0.1	0.83	0.97	0.05	1.03	0.05
NP_803421.1	2	acetyl-Coenzyme A acyltransferase 2 (mitochondrial 3-oxoacyl-Coenzyme A thiolase) [Mus musculus]	806.71		1.2	0.18	0.08	1	0.91	0.04	1.09	0.04
NP_031407.2	2	acetyl-Coenzyme A dehydrogenase, long-chain [Mus musculus]	730.49		0.88	-0.13	0.08	0.01	1.06	0.04	0.94	0.04
NP_031408.1	2	acetyl-Coenzyme A dehydrogenase, medium chain [Mus musculus]	474.11		1.08	0.08	0.14	0.88	0.96	0.07	1.04	0.07
NP_542364.1	2	aconitase 2, mitochondrial [Mus musculus]	1275.53		1	0	0.06	0.52	1	0.03	1	0.03
NP_032007.2	2	acyl-CoA synthetase long-chain family member 1 [Mus musculus]	488.25		1.15	0.14	0.11	0.98	0.93	0.05	1.07	0.05
NP_082252.1	2	acyl-CoA synthetase long-chain family member 5 [Mus musculus]	234.02	Membrane-WT-20070913	Membrane-WT-20070913	Membrane-WT-20070913	Membrane-WT-20070913	Membrane-WT-20070913				
NP_059062.1	2	acyl-Coenzyme A dehydrogenase, very long chain [Mus musculus]	1665.11		1.25	0.22	0.07	1	0.89	0.03	1.11	0.03
NP_000101.0	2	ALBU_BOVIN (P02769) Serum albumin precursor (Allergen Bos d 6) (BSA)	1518.29		0.9	-0.1	0.07	0	1.05	0.04	0.95	0.04
NP_904332.1	2	ATP synthase F0 subunit 8 [Mus musculus]	168.47		0.92	-0.08	0.1	0.06	1.04	0.05	0.96	0.05
NP_058054.2	2	ATP synthase, H+ transporting mitochondrial F1 complex, beta subunit [Mus musculus]	3570.95		1.01	0.01	0.03	0.78	0.99	0.02	1.01	0.02
NP_033855.2	2	ATP synthase, H+ transporting, mitochondrial F0 complex, subunit b, isoform 1 [Mus musculus]	566.83		0.98	-0.02	0.09	0.34	1.01	0.04	0.99	0.04
NP_082138.1	2	ATP synthase, H+ transporting, mitochondrial F0 complex, subunit d [Mus musculus]	1064.74		1.03	0.03	0.06	0.81	0.99	0.03	1.01	0.03
NP_058035.1	2	ATP synthase, H+ transporting, mitochondrial F0 complex, subunit F [Mus musculus]	270.62		1.02	0.02	0.13	0.63	0.99	0.07	1.01	0.07
NP_065607.1	2	ATP synthase, H+ transporting, mitochondrial F0 complex, subunit f, isoform 2 [Mus musculus]	99.12		0.97	-0.03	0.17	0.38	1.01	0.09	0.99	0.09
NP_031531.1	2	ATP synthase, H+ transporting, mitochondrial F1 complex, alpha subunit, isoform 1 [Mus musculus]	3436.11		1.04	0.04	0.03	0.95	0.98	0.02	1.02	0.02

NP_079589.1	2	ATP synthase, H+ transporting, mitochondrial F1 complex, delta subunit precursor [Mus musculus]	290.22	0.93	-0.07	0.1	0.05	1.03	0.05	0.97	0.05
NP_080259.1	2	ATP synthase, H+ transporting, mitochondrial F1 complex, epsilon subunit [Mus musculus]	115.91	1.01	0.01	0.12	0.6	0.99	0.06	1.01	0.06
NP_065640.1	2	ATP synthase, H+ transporting, mitochondrial F1 complex, gamma subunit [Mus musculus]	442.44	0.92	-0.08	0.09	0.05	1.04	0.04	0.96	0.04
NP_613063.1	2	ATP synthase, H+ transporting, mitochondrial F1 complex, O subunit [Mus musculus]	598	0.98	-0.02	0.06	0.24	1.01	0.03	0.99	0.03
NP_031557.1	2	B-cell receptor-associated protein 37 [Mus musculus]	291.71	0.95	-0.05	0.22	0.32	1.02	0.11	0.98	0.11
NP_031786.2	2	carnitine acetyltransferase [Mus musculus]	383.32	1.27	0.24	0.1	1	0.88	0.05	1.12	0.05
NP_034079.1	2	carnitine palmitoyltransferase 2 [Mus musculus]	539.29	1.46	0.38	0.16	1	0.81	0.08	1.19	0.08
NP_080720.1	2	citrate synthase [Mus musculus]	520.02	0.93	-0.07	0.1	0.08	1.04	0.05	0.96	0.05
NP_082221.1	2	citrate synthase-like protein [Mus musculus]	349.23	0.89	-0.12	0.13	0.04	1.06	0.06	0.94	0.06
NP_034027.1	2	creatine kinase, mitochondrial 1, ubiquitous [Mus musculus]	189.17	1.19	0.17	0.15	0.98	0.91	0.08	1.09	0.08
NP_940807.1	2	creatine kinase, mitochondrial 2 [Mus musculus]	1125.8	1.31	0.27	0.07	1	0.87	0.03	1.13	0.03
NP_904331.1	2	cytochrome c oxidase subunit II [Mus musculus]	623.63	1.06	0.06	0.08	0.93	0.97	0.04	1.03	0.04
NP_034071.1	2	cytochrome c oxidase subunit IV isoform 1 [Mus musculus]	540.31	0.92	-0.08	0.04	0	1.04	0.02	0.96	0.02
NP_031773.1	2	cytochrome c oxidase, subunit Va [Mus musculus]	441.94	1	0	0.07	0.56	1	0.04	1	0.04
NP_034072.1	2	cytochrome c oxidase, subunit Vb [Mus musculus]	238.62	1.05	0.05	0.1	0.86	0.97	0.05	1.03	0.05
NP_079904.1	2	cytochrome c oxidase, subunit VIb polypeptide 1 [Mus musculus]	357.74	0.95	-0.05	0.12	0.24	1.03	0.06	0.97	0.06
NP_444301.1	2	cytochrome c oxidase, subunit VIc [Mus musculus]	239.43	1	0	0.12	0.52	1	0.06	1	0.06
NP_034074.1	2	cytochrome c oxidase, subunit VIIa 1 [Mus musculus]	253.05	1	0	0.11	0.51	1	0.06	1	0.06
NP_031834.1	2	cytochrome c, somatic [Mus musculus]	318.58	1.15	0.14	0.13	0.98	0.93	0.06	1.07	0.06
NP_079843.1	2	cytochrome c-1 [Mus musculus]	351.45	1.15	0.14	0.09	1	0.93	0.04	1.07	0.04
NP_031887.2	2	dihydrolipoamide dehydrogenase [Mus musculus]	401.97	0.95	-0.05	0.16	0.2	1.02	0.08	0.98	0.08
NP_663589.2	2	dihydrolipoamide S-acetyltransferase (E2 component of pyruvate dehydrogenase complex) [Mus musculus]	617.75	0.84	-0.17	0.14	0.01	1.08	0.07	0.92	0.07
NP_084501.1	2	dihydrolipoamide S-succinyltransferase (E2 component of 2-oxo-glutarate complex) [Mus musculus]	420.2	0.84	-0.18	0.1	0	1.09	0.05	0.91	0.05
NP_034153.2	2	dodecenoyl-Coenzyme A delta isomerase (3,2 trans-enoyl-Coenyme A isomerase) [Mus musculus]	304.45	1.01	0.01	0.17	0.5	0.99	0.09	1.01	0.09
NP_663590.2	2	electron transferring flavoprotein, alpha polypeptide [Mus musculus]	564.68	1.03	0.03	0.09	0.71	0.98	0.05	1.02	0.05
NP_080971.2	2	electron transferring flavoprotein, beta polypeptide [Mus musculus]	761.25	1.01	0.01	0.09	0.54	1	0.05	1	0.05
NP_080070.1	2	electron transferring flavoprotein, dehydrogenase [Mus musculus]	911.73	1.16	0.15	0.08	1	0.92	0.04	1.08	0.04
NP_000202.0	2	ENO1_YEAST (P00924) Enolase 1 (EC 4.2.1.11) (2-phosphoglycerate dehydratase 1) (2-phospho-D-glycerate hydro-lyase 1)	541.65	0.91	-0.09	0.09	0	1.04	0.04	0.96	0.04
NP_444349.1	2	enoyl Coenzyme A hydratase, short chain, 1, mitochondrial [Mus musculus]	418.4	0.99	-0.01	0.15	0.44	1.01	0.07	0.99	0.07
NP_034339.1	2	fumarate hydratase 1 [Mus musculus]	347.48	1	0	0.18	0.54	1	0.09	1	0.09
NP_034455.1	2	glutamate oxaloacetate transaminase 2, mitochondrial [Mus musculus]	1105.3 4	1.09	0.09	0.05	1	0.96	0.03	1.04	0.03
NP_034611.1	2	heat shock protein 9A [Mus musculus]	520.72	0.79	-0.23	0.14	0.01	1.12	0.07	0.88	0.07
NP_058043.3	2	hydroxyacyl-Coenzyme A dehydrogenase type II [Mus musculus]	286.7	0.91	-0.09	0.2	0.25	1.04	0.1	0.96	0.1
NP_849209.1	2	hydroxyacyl-Coenzyme A dehydrogenase/3-ketoacyl-	1630.5	1.11	0.1	0.06	0.99	0.95	0.03	1.05	0.03

		Coenzyme A thiolase/enoyl-Coenzyme A hydratase (trifunctional protein), alpha subunit [Mus musculus]	8								
NP_663533.1	2	hydroxyacyl-Coenzyme A dehydrogenase/3-ketoacyl-Coenzyme A thiolase/enoyl-Coenzyme A hydratase (trifunctional protein), beta subunit [Mus musculus]	1098.01	1.32	0.28	0.06	1	0.86	0.03	1.14	0.03
NP_001028937.1	2	hypothetical protein LOC237880 [Mus musculus]	380.08	0.86	-0.15	0.13	0	1.07	0.06	0.93	0.06
NP_598768.1	2	hypothetical protein LOC52637 [Mus musculus]	100.29	1.27	0.24	0.36	0.92	0.88	0.16	1.12	0.16
NP_932096.1	2	hypothetical protein LOC66152 [Mus musculus]	158.9	0.94	-0.06	0.18	0.31	1.03	0.09	0.97	0.09
NP_080841.1	2	hypothetical protein LOC68117 [Mus musculus]	145.05	0.88	-0.13	0.26	0.22	1.07	0.13	0.93	0.13
NP_083949.2	2	inner membrane protein, mitochondrial [Mus musculus]	496.08	1	0	0.13	0.5	1	0.06	1	0.06
NP_766599.1	2	isocitrate dehydrogenase 2 (NADP+), mitochondrial [Mus musculus]	983.37	0.7	-0.35	0.09	0	1.18	0.04	0.82	0.04
NP_083849.1	2	isocitrate dehydrogenase 3 (NAD+) alpha [Mus musculus]	519.36	0.99	-0.01	0.1	0.44	1.01	0.05	0.99	0.05
NP_079628.1	2	low molecular mass ubiquinone-binding protein [Mus musculus]	247.08	0.97	-0.03	0.1	0.29	1.02	0.05	0.98	0.05
NP_032643.2	2	malate dehydrogenase 2, NAD (mitochondrial) [Mus musculus]	2239.45	1.07	0.07	0.05	0.99	0.97	0.03	1.03	0.03
NP_077159.1	2	NADH dehydrogenase (ubiquinone) 1 alpha subcomplex 10 [Mus musculus]	628.66	0.94	-0.06	0.13	0.2	1.03	0.06	0.97	0.06
NP_075801.1	2	NADH dehydrogenase (ubiquinone) 1 alpha subcomplex, 13 [Mus musculus]	279.03	0.9	-0.1	0.11	0.1	1.05	0.06	0.95	0.06
NP_035015.2	2	NADH dehydrogenase (ubiquinone) 1 alpha subcomplex, 2 [Mus musculus]	167.09	0.87	-0.14	0.17	0.06	1.07	0.09	0.93	0.09
NP_035016.1	2	NADH dehydrogenase (ubiquinone) 1 alpha subcomplex, 4 [Mus musculus]	475.85	0.94	-0.06	0.09	0.1	1.03	0.04	0.97	0.04
NP_075691.1	2	NADH dehydrogenase (ubiquinone) 1 alpha subcomplex, 7 (B14.5a) [Mus musculus]	154.3	0.92	-0.08	0.21	0.23	1.04	0.11	0.96	0.11
NP_080979.1	2	NADH dehydrogenase (ubiquinone) 1 alpha subcomplex, 8 [Mus musculus]	340.26	0.92	-0.08	0.16	0.19	1.04	0.08	0.96	0.08
NP_079634.1	2	NADH dehydrogenase (ubiquinone) 1 alpha subcomplex, 9 [Mus musculus]	806.81	0.89	-0.12	0.09	0.01	1.06	0.04	0.94	0.04
NP_080960.1	2	NADH dehydrogenase (ubiquinone) 1 beta subcomplex, 10 [Mus musculus]	384.37	0.97	-0.03	0.12	0.28	1.01	0.06	0.99	0.06
NP_075661.1	2	NADH dehydrogenase (ubiquinone) 1 beta subcomplex, 9 [Mus musculus]	228.67	0.9	-0.1	0.21	0.17	1.05	0.1	0.95	0.1
NP_077182.1	2	NADH dehydrogenase (ubiquinone) 1, subcomplex unknown, 2 [Mus musculus]	255.3	0.89	-0.12	0.15	0.06	1.06	0.07	0.94	0.07
NP_663493.1	2	NADH dehydrogenase (ubiquinone) Fe-S protein 1 [Mus musculus]	1608.61	0.9	-0.11	0.06	0	1.06	0.03	0.94	0.03
NP_694704.1	2	NADH dehydrogenase (ubiquinone) Fe-S protein 2 [Mus musculus]	537.15	0.96	-0.04	0.13	0.28	1.02	0.06	0.98	0.06
NP_080964.1	2	NADH dehydrogenase (ubiquinone) Fe-S protein 3 [Mus musculus]	597.97	0.94	-0.06	0.08	0.08	1.03	0.04	0.97	0.04
NP_035018.1	2	NADH dehydrogenase (ubiquinone) Fe-S protein 6 [Mus musculus]	304.24	0.85	-0.16	0.15	0.02	1.08	0.07	0.92	0.07
NP_659119.2	2	NADH dehydrogenase (ubiquinone) Fe-S protein 8 [Mus musculus]	232.04	0.95	-0.05	0.24	0.41	1.02	0.12	0.98	0.12
NP_598427.1	2	NADH dehydrogenase (ubiquinone) flavoprotein 1 [Mus musculus]	927.53	0.95	-0.05	0.07	0.07	1.03	0.04	0.97	0.04

NP_080886.1	2	NADH dehydrogenase 1 beta subcomplex 4 [Mus musculus]	302.68	0.94	-0.06	0.11	0.16	1.03	0.06	0.97	0.06
NP_062308.1	2	neuronal protein 15.6 [Mus musculus]	181.11	1.04	0.04	0.23	0.61	0.98	0.11	1.02	0.11
NP_032736.2	2	nicotinamide nucleotide transhydrogenase [Mus musculus]	1112.78	0.81	-0.21	0.08	0	1.11	0.04	0.89	0.04
NP_035086.2	2	oxoglutarate dehydrogenase (lipoamide) [Mus musculus]	1035.09	0.89	-0.12	0.12	0.04	1.06	0.06	0.94	0.06
NP_036151.1	2	peroxiredoxin 5 precursor [Mus musculus]	221.3	0.84	-0.18	0.27	0.1	1.09	0.13	0.91	0.13
XP_996295.1	2	PREDICTED: similar to acyl-CoA synthetase long-chain family member 1 isoform 2 [Mus musculus]	488.25	1.12	0.11	0.14	0.94	0.94	0.07	1.06	0.07
XP_996322.1	2	PREDICTED: similar to acyl-CoA synthetase long-chain family member 1 isoform 3 [Mus musculus]	221.57	1.06	0.06	0.15	0.72	0.97	0.07	1.03	0.07
XP_996347.1	2	PREDICTED: similar to acyl-CoA synthetase long-chain family member 1 isoform 4 [Mus musculus]	488.25	1.13	0.12	0.14	0.95	0.94	0.07	1.06	0.07
XP_996374.1	2	PREDICTED: similar to acyl-CoA synthetase long-chain family member 1 isoform 5 [Mus musculus]	488.25	1.13	0.12	0.12	0.96	0.94	0.06	1.06	0.06
XP_996193.1	2	PREDICTED: similar to ADP/ATP translocase 1 (Adenine nucleotide translocator 1) (ANT 1) (ADP,ATP carrier protein 1) (Solute carrier family 25 member 4) (ADP,ATP carrier protein, heart/skeletal muscle isoform T1) (mANC1) isoform 2 [Mus musculus]	1498.85	0.99	-0.01	0.04	0.28	1.01	0.02	0.99	0.02
XP_484885.2	2	PREDICTED: similar to ADP/ATP translocase 2 (Adenine nucleotide translocator 2) (ANT 2) (ADP,ATP carrier protein 2) (Solute carrier family 25 member 5) [Mus musculus]	573.17	1.03	0.03	0.09	0.71	0.99	0.05	1.01	0.05
XP_485652.2	2	PREDICTED: similar to ADP/ATP translocase 2 (Adenine nucleotide translocator 2) (ANT 2) (ADP,ATP carrier protein 2) (Solute carrier family 25 member 5) isoform 1 [Mus musculus]	520.89	0.97	-0.03	0.06	0.21	1.01	0.03	0.99	0.03
XP_909149.1	2	PREDICTED: similar to ADP/ATP translocase 2 (Adenine nucleotide translocator 2) (ANT 2) (ADP,ATP carrier protein 2) (Solute carrier family 25 member 5) isoform 1 [Mus musculus]	573.17	1.02	0.02	0.1	0.69	0.99	0.05	1.01	0.05
XP_923115.2	2	PREDICTED: similar to Aspartate aminotransferase, mitochondrial precursor (Transaminase A) (Glutamate oxaloacetate transaminase 2) [Mus musculus]	1038.76	1.07	0.07	0.06	0.99	0.96	0.03	1.04	0.03
XP_995005.1	2	PREDICTED: similar to ATP synthase B chain, mitochondrial precursor [Mus musculus]	268.07	0.98	-0.02	0.1	0.33	1.01	0.05	0.99	0.05
XP_997887.1	2	PREDICTED: similar to ATP synthase B chain, mitochondrial precursor [Mus musculus]	268.07	0.98	-0.02	0.09	0.38	1.01	0.05	0.99	0.05
XP_980826.1	2	PREDICTED: similar to ATP synthase coupling factor 6, mitochondrial precursor (ATPase subunit F6) [Mus musculus]	270.62	0.99	-0.01	0.11	0.39	1	0.06	1	0.06
XP_987162.1	2	PREDICTED: similar to ATP synthase gamma chain, mitochondrial precursor [Mus musculus]	591.93	0.93	-0.07	0.09	0.06	1.04	0.04	0.96	0.04
XP_918900.1	2	PREDICTED: similar to ATP synthase, H+ transporting, mitochondrial F0 complex, subunit d [Mus musculus]	356.6	1.03	0.03	0.13	0.69	0.98	0.07	1.02	0.07
XP_891471.1	2	PREDICTED: similar to ATP synthase, H+ transporting, mitochondrial F0 complex, subunit d [Mus musculus]	356.6	1.07	0.07	0.13	0.83	0.97	0.07	1.03	0.07
XP_999581.1	2	PREDICTED: similar to ATP synthase, H+ transporting, mitochondrial F0 complex, subunit f, isoform 2 [Mus musculus]	131.66	0.93	-0.07	0.21	0.16	1.04	0.1	0.96	0.1

XP_895476.1	2	PREDICTED: similar to ATP synthase, H+ transporting, mitochondrial F0 complex, subunit f, isoform 2 [Mus musculus]	131.66	0.95	-0.05	0.19	0.27	1.02	0.09	0.98	0.09
XP_998898.1	2	PREDICTED: similar to ATP synthase, H+ transporting, mitochondrial F1 complex, O subunit [Mus musculus]	398.66	0.94	-0.06	0.07	0.06	1.03	0.03	0.97	0.03
XP_484160.1	2	PREDICTED: similar to ATP synthase, H+ transporting, mitochondrial F1 complex, O subunit [Mus musculus]	398.66	0.95	-0.05	0.06	0.06	1.03	0.03	0.97	0.03
XP_911178.1	2	PREDICTED: similar to ATP synthase, H+ transporting, mitochondrial F1 complex, O subunit [Mus musculus]	398.66	0.95	-0.05	0.07	0.1	1.02	0.03	0.98	0.03
XP_994933.1	2	PREDICTED: similar to CG5903-PA [Mus musculus]	145.05	0.87	-0.14	0.28	0.17	1.07	0.14	0.93	0.14
XP_920836.1	2	PREDICTED: similar to cytochrome c oxidase, subunit VIc [Mus musculus]	176.99	0.98	-0.02	0.1	0.36	1.01	0.05	0.99	0.05
XP_999093.1	2	PREDICTED: similar to cytochrome c oxidase, subunit VIc [Mus musculus]	176.99	0.98	-0.02	0.11	0.36	1.01	0.06	0.99	0.06
XP_988746.1	2	PREDICTED: similar to cytochrome c oxidase, subunit VIc [Mus musculus]	176.99	0.99	-0.01	0.13	0.46	1	0.06	1	0.06
XP_996799.1	2	PREDICTED: similar to Cytochrome c, somatic [Mus musculus]	318.58	1.14	0.13	0.14	0.95	0.93	0.07	1.07	0.07
XP_987982.1	2	PREDICTED: similar to Cytochrome c, somatic [Mus musculus]	318.58	1.15	0.14	0.14	0.97	0.93	0.07	1.07	0.07
XP_980234.1	2	PREDICTED: similar to Cytochrome c, somatic isoform 1 [Mus musculus]	318.58	1.15	0.14	0.15	0.97	0.93	0.07	1.07	0.07
XP_980266.1	2	PREDICTED: similar to Cytochrome c, somatic isoform 2 [Mus musculus]	318.58	1.15	0.14	0.11	0.98	0.93	0.06	1.07	0.06
XP_914990.2	2	PREDICTED: similar to Electron transfer flavoprotein beta-subunit (Beta-ETF) [Mus musculus]	460.58	1.06	0.06	0.13	0.81	0.97	0.07	1.03	0.07
XP_00100311 8.1	2	PREDICTED: similar to electron transferring flavoprotein, beta polypeptide [Mus musculus]	622.18	1.01	0.01	0.1	0.52	1	0.05	1	0.05
XP_930842.1	2	PREDICTED: similar to hydroxyacyl-Coenzyme A dehydrogenase/3-ketoacyl-Coenzyme A thiolase/enoyl-Coenzyme A hydratase (trifunctional protein), beta subunit [Mus musculus]	1046.4 4	1.34	0.29	0.06	1	0.86	0.03	1.14	0.03
XP_987986.1	2	PREDICTED: similar to NADH dehydrogenase (ubiquinone) 1 alpha subcomplex, 9 [Mus musculus]	240.82	1.03	0.03	0.21	0.58	0.98	0.1	1.02	0.1
XP_990709.1	2	PREDICTED: similar to NADH dehydrogenase (ubiquinone) 1, subcomplex unknown, 2 [Mus musculus]	255.3	0.89	-0.12	0.14	0.07	1.06	0.07	0.94	0.07
XP_894449.1	2	PREDICTED: similar to NADH dehydrogenase (ubiquinone) Fe-S protein 3 [Mus musculus]	537.67	0.9	-0.1	0.11	0.05	1.05	0.05	0.95	0.05
XP_894909.1	2	PREDICTED: similar to NADH dehydrogenase (ubiquinone) Fe-S protein 6 [Mus musculus]	278.57	0.81	-0.21	0.15	0	1.1	0.07	0.9	0.07
XP_909811.1	2	PREDICTED: similar to NADH dehydrogenase (ubiquinone) Fe-S protein 6 [Mus musculus]	113.76	0.98	-0.02	0.3	0.43	1.01	0.15	0.99	0.15
XP_987021.1	2	PREDICTED: similar to NADH-ubiquinone oxidoreductase 24 kDa subunit, mitochondrial precursor isoform 1 [Mus musculus]	514.82	1.09	0.09	0.09	0.94	0.96	0.05	1.04	0.05
XP_987060.1	2	PREDICTED: similar to NADH-ubiquinone oxidoreductase 24 kDa subunit, mitochondrial precursor isoform 2 [Mus musculus]	574.55	1.07	0.07	0.09	0.93	0.97	0.05	1.03	0.05
XP_922851.1	2	PREDICTED: similar to NADH-ubiquinone oxidoreductase 24 kDa subunit, mitochondrial precursor isoform 3 [Mus	574.55	1.06	0.06	0.1	0.94	0.97	0.05	1.03	0.05

		musculus]										
XP_978921.1	2	PREDICTED: similar to prohibitin [Mus musculus]	646.12		0.93	-0.07	0.1	0.11	1.04	0.05	0.96	0.05
XP_979065.1	2	PREDICTED: similar to prohibitin [Mus musculus]	646.12		0.93	-0.07	0.11	0.18	1.04	0.05	0.96	0.05
XP_983153.1	2	PREDICTED: similar to prohibitin [Mus musculus]	646.12		0.93	-0.07	0.11	0.12	1.04	0.05	0.96	0.05
XP_981174.1	2	PREDICTED: similar to pyruvate dehydrogenase (lipoamide) beta [Mus musculus]	377.78		0.9	-0.11	0.14	0.07	1.06	0.07	0.94	0.07
XP_996141.1	2	PREDICTED: similar to solute carrier family 25, member 4 isoform 1 [Mus musculus]	1295.9		0.98	-0.02	0.04	0.25	1.01	0.02	0.99	0.02
XP_896808.2	2	PREDICTED: similar to Stress-70 protein, mitochondrial precursor (75 kDa glucose-regulated protein) (GRP 75) (Peptide-binding protein 74) (PBP74) (P66 MOT) (Mortalin) [Mus musculus]	275.35	Membrane-WT-20070913	Membrane-WT-20070913	Membrane-WT-20070913	Membrane-WT-20070913	Membrane-WT-20070913				
XP_998318.1	2	PREDICTED: similar to Stress-70 protein, mitochondrial precursor (75 kDa glucose-regulated protein) (GRP 75) (Peptide-binding protein 74) (PBP74) (P66 MOT) (Mortalin) [Mus musculus]	258.3	Membrane-WT-20070913	Membrane-WT-20070913	Membrane-WT-20070913	Membrane-WT-20070913	Membrane-WT-20070913				
XP_134169.3	2	PREDICTED: solute carrier family 25 (mitochondrial carrier, adenine nucleotide translocator), member 4 isoform 1 [Mus musculus]	1498.85		0.99	-0.01	0.04	0.32	1.01	0.02	0.99	0.02
XP_902025.1	2	PREDICTED: solute carrier family 25 (mitochondrial carrier, adenine nucleotide translocator), member 4 isoform 2 [Mus musculus]	1295.9		0.97	-0.03	0.05	0.15	1.01	0.02	0.99	0.02
NP_032857.1	2	prohibitin [Mus musculus]	646.12		0.92	-0.08	0.12	0.1	1.04	0.06	0.96	0.06
NP_077183.1	2	pyruvate dehydrogenase (lipoamide) beta [Mus musculus]	400.22		0.89	-0.12	0.12	0.01	1.06	0.06	0.94	0.06
NP_077173.1	2	solute carrier family 25 (mitochondrial carrier oxoglutarate carrier), member 11 [Mus musculus]	419.78		0.96	-0.04	0.12	0.27	1.02	0.06	0.98	0.06
NP_056644.1	2	solute carrier family 25 (mitochondrial carrier, adenine nucleotide translocator), member 13 [Mus musculus]	427.52		0.86	-0.15	0.14	0.02	1.07	0.07	0.93	0.07
NP_766024.1	2	solute carrier family 25 (mitochondrial carrier, Aralar), member 12 [Mus musculus]	666.47		0.96	-0.04	0.15	0.28	1.02	0.07	0.98	0.07
NP_598429.1	2	solute carrier family 25 (mitochondrial carrier, phosphate carrier), member 3 [Mus musculus]	635.68		0.93	-0.07	0.06	0.02	1.04	0.03	0.96	0.03
NP_848473.1	2	solute carrier family 25 (mitochondrial carrier; adenine nucleotide translocator), member 31 [Mus musculus]	292.91		0.93	-0.07	0.17	0.22	1.03	0.09	0.97	0.09
NP_031477.1	2	solute carrier family 25, member 5 [Mus musculus]	1141.9		0.95	-0.05	0.05	0.03	1.02	0.03	0.98	0.03
NP_075770.1	2	succinate dehydrogenase Fp subunit [Mus musculus]	1508.45		0.96	-0.04	0.07	0.1	1.02	0.03	0.98	0.03
NP_063932.1	2	succinate-CoA ligase, GDP-forming, alpha subunit [Mus musculus]	334.92		0.92	-0.08	0.21	0.2	1.04	0.1	0.96	0.1
NP_035636.1	2	succinate-Coenzyme A ligase, ADP-forming, beta subunit [Mus musculus]	178.01		0.87	-0.14	0.2	0.12	1.07	0.1	0.93	0.1
NP_766333.1	2	Tu translation elongation factor, mitochondrial [Mus musculus]	434.84		0.83	-0.19	0.18	0.02	1.1	0.09	0.9	0.09
NP_080175.1	2	ubiquinol cytochrome c reductase core protein 2 [Mus musculus]	1503.34		1.06	0.06	0.04	1	0.97	0.02	1.03	0.02
NP_080495.1	2	ubiquinol-cytochrome c reductase binding protein [Mus musculus]	368.49		0.98	-0.02	0.13	0.38	1.01	0.06	0.99	0.06
NP_079683.2	2	ubiquinol-cytochrome c reductase core protein 1 [Mus	1776.7		1.01	0.01	0.06	0.56	1	0.03	1	0.03

		musculus]	9								
NP_079986.1	2	ubiquinol-cytochrome c reductase, Rieske iron-sulfur polypeptide 1 [Mus musculus]	882.78	1	0	0.06	0.39	1	0.03	1	0.03
NP_075700.2	2	upregulated during skeletal muscle growth 5 [Mus musculus]	239.24	1.03	0.03	0.15	0.73	0.98	0.07	1.02	0.07
NP_035824.1	2	voltage-dependent anion channel 1 [Mus musculus]	1061.6 9	1.05	0.05	0.09	0.85	0.97	0.04	1.03	0.04
NP_035825.1	2	voltage-dependent anion channel 2 [Mus musculus]	719.86	1	0	0.1	0.46	1	0.05	1	0.05
NP_035826.1	2	voltage-dependent anion channel 3 [Mus musculus]	319.85	1.06	0.06	0.12	0.84	0.97	0.06	1.03	0.06

Supplemental Table S2B. Proteomic Analysis of all Mitochondrial Matrix Proteins from CIRKO Mice.

Accession	OK	Description	Score	Unique	Matrix-WT-20070913:Matrix-TG-20070913_Ratio	Matrix-WT-20070913:Matrix-TG-20070913_Log(e) Ratio	Matrix-WT-20070913:Matrix-TG-20070913_Log(e) StdDev	Matrix-WT-20070913:Matrix-TG-20070913__P	Matrix-TG-20070913_Rel Profile	Matrix-TG-20070913_Rel Profile SD	Matrix-WT-20070913_Rel Profile	Matrix-WT-20070913_Rel Profile SD
NP_080448.1	2	2,4-dienoyl CoA reductase 1, mitochondrial [Mus musculus]	470		0.94	-0.06	0.26	0.34	1.03	0.13	0.97	0.13
NP_663542.1	2	3-hydroxyisobutyrate dehydrogenase, mitochondrial precursor [Mus musculus]	398		0.93	-0.07	0.25	0.31	1.04	0.12	0.96	0.12
NP_666220.1	2	3-hydroxyisobutyryl-Coenzyme A hydrolase [Mus musculus]	241		0.95	-0.05	0.28	0.4	1.02	0.14	0.98	0.14
NP_077150.1	2	3-oxoacid CoA transferase 1 [Mus musculus]	1715		0.81	-0.21	0.1	0	1.1	0.05	0.9	0.05
NP_542142.1	2	acetyl-CoA synthetase 2-like [Mus musculus]	507		0.95	-0.05	0.18	0.3	1.02	0.09	0.98	0.09
NP_659033.1	2	acetyl-Coenzyme A acetyltransferase 1 precursor [Mus musculus]	1484		1.01	0.01	0.08	0.52	1	0.04	1	0.04
NP_803421.1	2	acetyl-Coenzyme A acyltransferase 2 (mitochondrial 3-oxoacyl-Coenzyme A thiolase) [Mus musculus]	2650		1.35	0.3	0.06	1	0.85	0.03	1.15	0.03
NP_031407.2	2	acetyl-Coenzyme A dehydrogenase, long-chain [Mus musculus]	1660		1.12	0.11	0.06	1	0.94	0.03	1.06	0.03
NP_031408.1	2	acetyl-Coenzyme A dehydrogenase, medium chain [Mus musculus]	1342		1.31	0.27	0.06	1	0.87	0.03	1.13	0.03
NP_542364.1	2	aconitase 2, mitochondrial [Mus musculus]	4681		1.09	0.09	0.03	1	0.95	0.02	1.05	0.02
NP_031409.2	2	acyl-Coenzyme A dehydrogenase, short chain [Mus musculus]	942		1.4	0.34	0.15	1	0.83	0.07	1.17	0.07
NP_059062.1	2	acyl-Coenzyme A dehydrogenase, very long chain [Mus musculus]	1180		0.66	-0.42	0.18	0	1.21	0.09	0.79	0.09
NP_067274.1	2	adenylate kinase 3 [Mus musculus]	241		0.96	-0.04	0.39	0.47	1.02	0.19	0.98	0.19
NP_000101.0	2	ALBU_BOVIN (P02769) Serum albumin precursor (Allergen Bos d 6) (BSA)	1496		0.72	-0.33	0.09	0	1.16	0.04	0.84	0.04
NP_033786.1	2	aldehyde dehydrogenase 2, mitochondrial [Mus musculus]	689		1	0	0.2	0.46	1	0.1	1	0.1
NP_780647.2	2	aldehyde dehydrogenase 4 family, member A1 [Mus musculus]	301	Matrix-WT-20070913	Matrix-WT-20070913	Matrix-WT-20070913	Matrix-WT-20070913	Matrix-WT-20070913				
NP_598803.1	2	aldehyde dehydrogenase family 6, subfamily A1 [Mus musculus]	508		1.21	0.19	0.13	1	0.91	0.06	1.09	0.06
NP_058054.2	2	ATP synthase, H+ transporting mitochondrial F1 complex, beta subunit [Mus musculus]	537		0.73	-0.31	0.21	0	1.15	0.11	0.85	0.11
NP_031531.1	2	ATP synthase, H+ transporting, mitochondrial F1 complex, alpha subunit, isoform 1 [Mus musculus]	444		0.73	-0.31	0.24	0	1.15	0.12	0.85	0.12
NP_033867.1	2	branched chain aminotransferase 2, mitochondrial [Mus musculus]	358		1.09	0.09	0.18	0.82	0.95	0.09	1.05	0.09
NP_083832.1	2	citrate lyase beta like [Mus musculus]	210		1.07	0.07	0.3	0.69	0.97	0.15	1.03	0.15

NP_080720.1	2	citrate synthase [Mus musculus]	996	1.11	0.1	0.06	1	0.95	0.03	1.05	0.03
NP_082221.1	2	citrate synthase-like protein [Mus musculus]	581	1.02	0.02	0.07	0.61	0.99	0.04	1.01	0.04
NP_036136.1	2	cytosolic acyl-CoA thioesterase 1 [Mus musculus]	282	1.15	0.14	0.2	0.9	0.93	0.1	1.07	0.1
NP_031887.2	2	dihydrolipoamide dehydrogenase [Mus musculus]	1109	0.99	-0.01	0.09	0.42	1	0.05	1	0.05
NP_663589.2	2	dihydrolipoamide S-acetyltransferase (E2 component of pyruvate dehydrogenase complex) [Mus musculus]	785	1.03	0.03	0.13	0.66	0.98	0.06	1.02	0.06
NP_084501.1	2	dihydrolipoamide S-succinyltransferase (E2 component of 2-oxo-glutarate complex) [Mus musculus]	677	1.07	0.07	0.14	0.84	0.97	0.07	1.03	0.07
NP_034153.2	2	dodecenoyl-Coenzyme A delta isomerase (3,2 trans-enoyl-Coenyme A isomerase) [Mus musculus]	787	1.3	0.26	0.1	1	0.87	0.05	1.13	0.05
NP_663590.2	2	electron transferring flavoprotein, alpha polypeptide [Mus musculus]	1585	1.12	0.11	0.08	1	0.94	0.04	1.06	0.04
NP_080971.2	2	electron transferring flavoprotein, beta polypeptide [Mus musculus]	1329	1.06	0.06	0.06	0.97	0.97	0.03	1.03	0.03
NP_000202.0	2	ENO1_YEAST (P00924) Enolase 1 (EC 4.2.1.11) (2-phosphoglycerate dehydratase 1) (2-phospho-D-glycerate hydro-lyase 1)	515	0.58	-0.54	0.14	0	1.26	0.06	0.74	0.06
NP_058052.1	2	enoyl coenzyme A hydratase 1, peroxisomal [Mus musculus]	279	1.03	0.03	0.24	0.59	0.98	0.12	1.02	0.12
NP_444349.1	2	enoyl Coenzyme A hydratase, short chain, 1, mitochondrial [Mus musculus]	726	1.14	0.13	0.11	0.99	0.94	0.06	1.06	0.06
NP_613067.1	2	es1 protein [Mus musculus]	615	0.97	-0.03	0.1	0.24	1.02	0.05	0.98	0.05
NP_034339.1	2	fumarate hydratase 1 [Mus musculus]	1166	1.09	0.09	0.1	0.97	0.95	0.05	1.05	0.05
NP_032159.1	2	glutamate dehydrogenase 1 [Mus musculus]	444	0.93	-0.07	0.46	0.39	1.03	0.22	0.97	0.22
NP_034455.1	2	glutamate oxaloacetate transaminase 2, mitochondrial [Mus musculus]	1385	1.14	0.13	0.07	1	0.93	0.03	1.07	0.03
NP_032329.1	2	heat shock protein 1 (chaperonin 10) [Mus musculus]	381	0.93	-0.07	0.15	0.14	1.04	0.07	0.96	0.07
NP_034607.2	2	heat shock protein 1 (chaperonin) [Mus musculus]	387	1.21	0.19	0.24	0.93	0.91	0.12	1.09	0.12
NP_034611.1	2	heat shock protein 9A [Mus musculus]	1171	1	0	0.09	0.53	1	0.05	1	0.05
NP_058043.3	2	hydroxyacyl-Coenzyme A dehydrogenase type II [Mus musculus]	313	1.06	0.06	0.26	0.68	0.97	0.13	1.03	0.13
NP_849209.1	2	hydroxyacyl-Coenzyme A dehydrogenase/3-ketoacyl-Coenzyme A thiolase/enoyl-Coenzyme A hydratase (trifunctional protein), alpha subunit [Mus musculus]	1483	1.04	0.04	0.11	0.81	0.98	0.05	1.02	0.05
NP_663533.1	2	hydroxyacyl-Coenzyme A dehydrogenase/3-ketoacyl-Coenzyme A thiolase/enoyl-Coenzyme A hydratase (trifunctional protein), beta subunit [Mus musculus]	753	0.73	-0.31	0.21	0	1.15	0.1	0.85	0.1
NP_083949.2	2	inner membrane protein, mitochondrial [Mus musculus]	600	0.78	-0.25	0.18	0.01	1.13	0.09	0.87	0.09
NP_766599.1	2	isocitrate dehydrogenase 2 (NADP+), mitochondrial [Mus musculus]	2469	0.94	-0.06	0.05	0.03	1.03	0.03	0.97	0.03
NP_083849.1	2	isocitrate dehydrogenase 3 (NAD+) alpha [Mus musculus]	853	1.28	0.25	0.08	1	0.88	0.04	1.12	0.04
NP_062800.1	2	isovaleryl coenzyme A dehydrogenase [Mus musculus]	377	1.02	0.02	0.29	0.54	0.99	0.14	1.01	0.14
NP_032238.1	2	L-3-hydroxyacyl-Coenzyme A dehydrogenase, short chain [Mus musculus]	549	1.43	0.36	0.11	1	0.82	0.05	1.18	0.05
NP_032643.2	2	malate dehydrogenase 2, NAD (mitochondrial) [Mus musculus]	2730	0.97	-0.03	0.04	0.09	1.02	0.02	0.98	0.02
NP_598949.2	2	mitochondrial acyl-CoA thioesterase 1 [Mus musculus]	397	1.16	0.15	0.21	0.91	0.93	0.1	1.07	0.1
NP_035086.2	2	oxoglutarate dehydrogenase (lipoamide) [Mus musculus]	1687	1.3	0.26	0.09	1	0.87	0.04	1.13	0.04
NP_031478.1	2	peroxiredoxin 3 [Mus musculus]	473	1.04	0.04	0.14	0.8	0.98	0.07	1.02	0.07
NP_036151.1	2	peroxiredoxin 5 precursor [Mus musculus]	974	0.98	-0.02	0.1	0.34	1.01	0.05	0.99	0.05

XP_143732.3	2	PREDICTED: histidine triad nucleotide binding protein 2 [Mus musculus]	171	1.02	0.02	0.31	0.52	0.99	0.16	1.01	0.16
XP_898273.1	2	PREDICTED: similar to 10 kDa heat shock protein, mitochondrial (Hsp10) (10 kDa chaperonin) (CPN10) [Mus musculus]	352	0.9	-0.11	0.16	0.12	1.05	0.08	0.95	0.08
XP_995914.1	2	PREDICTED: similar to 10 kDa heat shock protein, mitochondrial (Hsp10) (10 kDa chaperonin) (CPN10) [Mus musculus]	352	0.9	-0.1	0.16	0.13	1.05	0.08	0.95	0.08
XP_916456.1	2	PREDICTED: similar to 10 kDa heat shock protein, mitochondrial (Hsp10) (10 kDa chaperonin) (CPN10) [Mus musculus]	352	0.91	-0.09	0.16	0.19	1.05	0.08	0.95	0.08
XP_989864.1	2	PREDICTED: similar to 3-hydroxyisobutyrate dehydrogenase, mitochondrial precursor [Mus musculus]	270	0.97	-0.03	0.37	0.43	1.01	0.18	0.99	0.18
XP_996439.1	2	PREDICTED: similar to 3-hydroxyisobutyrate dehydrogenase, mitochondrial precursor [Mus musculus]	198	0.98	-0.02	0.36	0.46	1.01	0.18	0.99	0.18
XP_916687.1	2	PREDICTED: similar to 3-hydroxyisobutyrate dehydrogenase, mitochondrial precursor [Mus musculus]	261	1.03	0.03	0.38	0.56	0.99	0.19	1.01	0.19
XP_484008.1	2	PREDICTED: similar to 60 kDa heat shock protein, mitochondrial precursor (Hsp60) (60 kDa chaperonin) (CPN60) (Heat shock protein 60) (HSP-60) (Mitochondrial matrix protein P1) (HSP-65) [Mus musculus]	392	1.2	0.18	0.26	0.93	0.91	0.13	1.09	0.13
XP_981087.1	2	PREDICTED: similar to 60 kDa heat shock protein, mitochondrial precursor (Hsp60) (60 kDa chaperonin) (CPN60) (Heat shock protein 60) (HSP-60) (Mitochondrial matrix protein P1) (HSP-65) [Mus musculus]	392	1.25	0.22	0.21	0.97	0.89	0.1	1.11	0.1
XP_980447.1	2	PREDICTED: similar to Acyl-coenzyme A thioesterase 1 (Acyl-CoA thioesterase 1) (Inducible cytosolic acyl-coenzyme A thioester hydrolase) (Long chain acyl-CoA thioester hydrolase) (Long chain acyl-CoA hydrolase) (CTE-I) [Mus musculus]	286	1.12	0.11	0.19	0.83	0.94	0.1	1.06	0.1
XP_923115.2	2	PREDICTED: similar to Aspartate aminotransferase, mitochondrial precursor (Transaminase A) (Glutamate oxaloacetate transaminase 2) [Mus musculus]	1351	1.14	0.13	0.09	1	0.93	0.04	1.07	0.04
XP_995088.1	2	PREDICTED: similar to coiled-coil-helix-coiled-coil-helix domain containing 3 isoform 2 [Mus musculus]	246	0.78	-0.25	0.23	0	1.12	0.12	0.88	0.12
XP_914990.2	2	PREDICTED: similar to Electron transfer flavoprotein beta-subunit (Beta-ETF) [Mus musculus]	930	1.06	0.06	0.09	0.86	0.97	0.04	1.03	0.04
XP_001003118.1	2	PREDICTED: similar to electron transferring flavoprotein, beta polypeptide [Mus musculus]	1000	1.05	0.05	0.06	0.94	0.97	0.03	1.03	0.03
XP_992848.1	2	PREDICTED: similar to Glutamate dehydrogenase 1, mitochondrial precursor (GDH) isoform 2 [Mus musculus]	404	1.12	0.11	0.38	0.78	0.95	0.18	1.05	0.18
XP_992813.1	2	PREDICTED: similar to Glutamate dehydrogenase 1, mitochondrial precursor (GDH) isoform 3 [Mus musculus]	320	1.13	0.12	0.41	0.69	0.94	0.2	1.06	0.2
XP_909681.2	2	PREDICTED: similar to Histidine triad nucleotide-binding protein 2 (HINT-2) (HINT-3) [Mus musculus]	171	0.98	-0.02	0.24	0.48	1.01	0.12	0.99	0.12
XP_978522.1	2	PREDICTED: similar to Histidine triad nucleotide-binding protein 2 (HINT-2) (HINT-3) [Mus musculus]	171	1	0	0.33	0.48	1	0.16	1	0.16
XP_930842.1	2	PREDICTED: similar to hydroxyacyl-Coenzyme A dehydrogenase/3-ketoacyl-Coenzyme A thiolase/enoyl-Coenzyme A hydratase (trifunctional protein), beta subunit	704	0.75	-0.29	0.22	0	1.14	0.11	0.86	0.11

		[Mus musculus]										
XP_001001780.1	2	PREDICTED: similar to Malate dehydrogenase, mitochondrial precursor [Mus musculus]	179		1.14	0.13	0.15	0.93	0.94	0.07	1.06	0.07
XP_982094.1	2	PREDICTED: similar to Malate dehydrogenase, mitochondrial precursor [Mus musculus]	179		1.15	0.14	0.15	0.95	0.93	0.07	1.07	0.07
XP_989435.1	2	PREDICTED: similar to Malate dehydrogenase, mitochondrial precursor [Mus musculus]	179		1.15	0.14	0.13	0.99	0.93	0.07	1.07	0.07
XP_988293.1	2	PREDICTED: similar to oxoglutarate dehydrogenase-like [Mus musculus]	589	Matrix-WT-20070913	Matrix-WT-20070913	Matrix-WT-20070913	Matrix-WT-20070913	Matrix-WT-20070913				
XP_138959.5	2	PREDICTED: similar to oxoglutarate dehydrogenase-like isoform 1 [Mus musculus]	589	Matrix-WT-20070913	Matrix-WT-20070913	Matrix-WT-20070913	Matrix-WT-20070913	Matrix-WT-20070913				
XP_991516.1	2	PREDICTED: similar to oxoglutarate dehydrogenase-like isoform 1 [Mus musculus]	589	Matrix-WT-20070913	Matrix-WT-20070913	Matrix-WT-20070913	Matrix-WT-20070913	Matrix-WT-20070913				
XP_991547.1		PREDICTED: similar to oxoglutarate dehydrogenase-like isoform 2 [Mus musculus]	589	Matrix-WT-20070913	Matrix-WT-20070913	Matrix-WT-20070913	Matrix-WT-20070913	Matrix-WT-20070913				
XP_991579.1		PREDICTED: similar to oxoglutarate dehydrogenase-like isoform 3 [Mus musculus]	589	Matrix-WT-20070913	Matrix-WT-20070913	Matrix-WT-20070913	Matrix-WT-20070913	Matrix-WT-20070913				
XP_991618.1		PREDICTED: similar to oxoglutarate dehydrogenase-like isoform 4 [Mus musculus]	610	Matrix-WT-20070913	Matrix-WT-20070913	Matrix-WT-20070913	Matrix-WT-20070913	Matrix-WT-20070913				
XP_981174.1		PREDICTED: similar to pyruvate dehydrogenase (lipoamide) beta [Mus musculus]	616		1.09	0.09	0.12	0.93	0.95	0.06	1.05	0.06
XP_986100.1		PREDICTED: similar to Pyruvate dehydrogenase E1 component alpha subunit, somatic form, mitochondrial precursor (PDHE1-A type I) isoform 2 [Mus musculus]	654		1.32	0.28	0.12	1	0.86	0.06	1.14	0.06
XP_998318.1		PREDICTED: similar to Stress-70 protein, mitochondrial precursor (75 kDa glucose-regulated protein) (GRP 75) (Peptide-binding protein 74) (PBP74) (P66 MOT) (Mortalin) [Mus musculus]	406		0.97	-0.03	0.21	0.38	1.02	0.1	0.98	0.1
XP_896808.2		PREDICTED: similar to Stress-70 protein, mitochondrial precursor (75 kDa glucose-regulated protein) (GRP 75) (Peptide-binding protein 74) (PBP74) (P66 MOT) (Mortalin) [Mus musculus]	366		1.02	0.02	0.16	0.59	0.99	0.08	1.01	0.08
NP_036149.1		programmed cell death 8 [Mus musculus]	309		0.87	-0.14	0.27	0.14	1.07	0.13	0.93	0.13
NP_077183.1		pyruvate dehydrogenase (lipoamide) beta [Mus musculus]	847		1.16	0.15	0.12	1	0.93	0.06	1.07	0.06
NP_032836.1		pyruvate dehydrogenase E1 alpha 1 [Mus musculus]	654		1.34	0.29	0.11	1	0.86	0.05	1.14	0.05

NP_063932.1	succinate-CoA ligase, GDP-forming, alpha subunit [Mus musculus]	443	Matrix-WT-20070913	Matrix-WT-20070913	Matrix-WT-20070913	Matrix-WT-20070913	Matrix-WT-20070913				
NP_035636.1	succinate-Coenzyme A ligase, ADP-forming, beta subunit [Mus musculus]	478		1.65	0.5	0.14	1	0.75	0.06	1.25	0.06
NP_038699.2	superoxide dismutase 2, mitochondrial [Mus musculus]	801		1.02	0.02	0.11	0.63	0.99	0.06	1.01	0.06
NP_080066.1	thioesterase superfamily member 2 [Mus musculus]	165		1.7	0.53	0.26	1	0.74	0.12	1.26	0.12
NP_766333.1	Tu translation elongation factor, mitochondrial [Mus musculus]	443		0.83	-0.19	0.24	0.09	1.09	0.12	0.91	0.12

SUPPLEMENTAL FIGURES AND LEGENDS

SUPPLEMENTAL FIGURE S1. Purity of mitochondrial subfractions.

- **A)** Protein content of the matrix protein MnSOD and the inner mitochondrial membrane protein complex IV subunit 4 in whole mitochondrial fraction (WMF), mitochondrial matrix (MT), and mitochondrial membranes (MB).
- **B)** Protein content of the outer mitochondrial membrane protein mitofusin 2 (Mfn2) in mitochondrial matrix and membrane fractions.

SUPPLEMENTAL FIGURE S2. Contractile parameters and MVO_2 under low and high calcium conditions.

A) Left ventricular developed pressure (LVDVP) at baseline (2 mmol/L extracellular calcium concentrations) and following calcium-induced inotropic stress (4 mmol/L extracellular calcium concentrations) in 8 week-old Langendorff-perfused CIRKO (black bars) and wild-type (open bars) hearts.

B) Same as **A** for rate pressure product (RPP)

C) Same as **A** for dP/dt_{min} and dP/dt_{max}

D) Same as **A** for myocardial oxygen consumption (MVO_2)

Data are means ± SEM. * $p < 0.05$; ** $p < 0.005$ vs. equivalently treated wild-type controls. # $p<0.05$; ## $p<0.005$ vs. 2mM Ca^{2+}

SUPPLEMENTAL FIGURE S3. Maximal electron transport chain capacity in isolated mitochondria from 24 week-old wild-type and CIRKO mice.

(A) and **(B)** respiration traces of isolated mitochondria (0.4 mg/ml) from hearts of 24 week-old wild-type and CIRKO mice respectively. Respirations were carried in the presence of pyruvate-malate. Uncoupling of the electron transport chain was achieved by addition of FCCP (carbonyl cyanide p-trifluoromethoxyphenylhydrazone).

(C) Summary of states of respiration as detailed above in wild-type (n = 4) and CIRKO (n=4).

SUPPLEMENTAL FIGURE S4. Age-dependent decline in mitochondrial enzyme activities.

A) Fold change in citrate synthase (CS) activity in 8 (five per group), 24 (four to five per group) and 54 (three per group) week-old CIRKO (black bars) and wild-type (white bars). Each value represents fold change in CS activity in CIRKO mice relative to wild-type mice, which is arbitrarily defined as 1. Statistics: Wild-type (WT) vs. CIRKO, $p<0.04$ at 24 and 54-weeks.

B) Fold changes in Carnitine palmitoyl-transferase 1 (CPT1) activity in 8 (seven per group), 24 (four to six per group) and 54 (five to six per group) week-old CIRKO (black bars) and wild-type (white bars). Each value represents fold change in CPT1 activity in CIRKO mice relative to that in wild-type mice, which is arbitrarily defined as 1. Statistics: WT vs. CIRKO, $p<0.01$ at 8 and 54-weeks.

C) Fold changes in 3-Hydroxyacyl-CoA dehydrogenase (HADH) activity in 8 (five per group), 24 (four to five per group) and 54 (three per group) week-old CIRKO (black bars) and wild-type (white bars). Each value represents fold change in HADH activity in

CIRKO mice relative to wild-type mice, which is arbitrarily defined as 1. Statistics: WT vs. CIRKO, $p<0.05$ at 8 and 54-weeks.

SUPPLEMENTAL FIGURE S5. Age-related changes in gene expression in wild-types (open circles) and CIRKO (filled circles), at 3, 8 and 24-weeks.

SUPPLEMENTAL FIGURE S6. PDHE1α protein expression in 14 week-old male wild-type and CIRKO mice.

- **A)** Upper panel represents phospo-PDHE1α and lower panel is total PDHE1α expression in whole heart homogenates of 6 wild-types and 4 CIRKO mice.
- **B)** Densitometric analysis. Phosphorylation state was normalized to total PDHE1α and data represent fold change versus WT considered as 1.

SUPPLEMENTAL FIGURE S7. IGF1-Receptor expression and insulin signaling in 8 week-old wild-type and CIRKO mice. WT and CIRKO hearts were perfused or not with 1 nM insulin.

A) *Upper panel*, IGF1-Receptor expression in WT and CIRKO whole heart homogenates. *Lower panel*, densitometric analysis. IGF1-R expression was normalized to Coomassie blue staining (CB). n=7-8 per group.

B) and **C)** Phospho-AKT-Ser^{473} and Phospho-GSK3β-Ser^{9} immunoblotting and respective densitometric analysis. Phosphorylation state was normalized to total AKT or total GSK3β expression, respectively. n=3-4 per group. $^{\#,*}$ $p<0.05$ compared to WT or WT basal respectively.

SUPPLEMENTAL FIGURE S8. Palmitate oxidation **(A)**, Oxygen consumption **(B)** and cardiac efficiency **(C)** in isolated-working hearts from 8 week-old CIRKO and wild-type mice. * $p < 0.05$; ** $p < 0.005$ vs. age-matched wild-type controls

SUPPLEMENTAL FIGURE S1

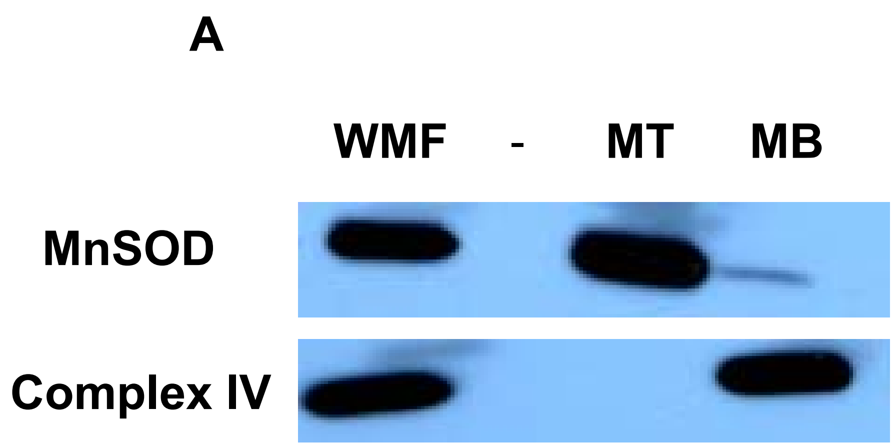

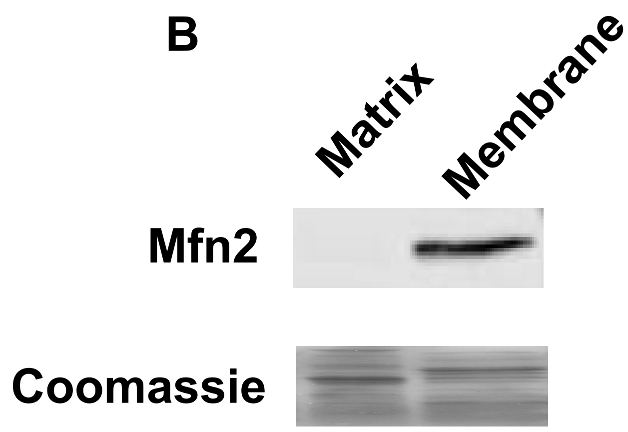

SUPPLEMENTAL FIGURE S2

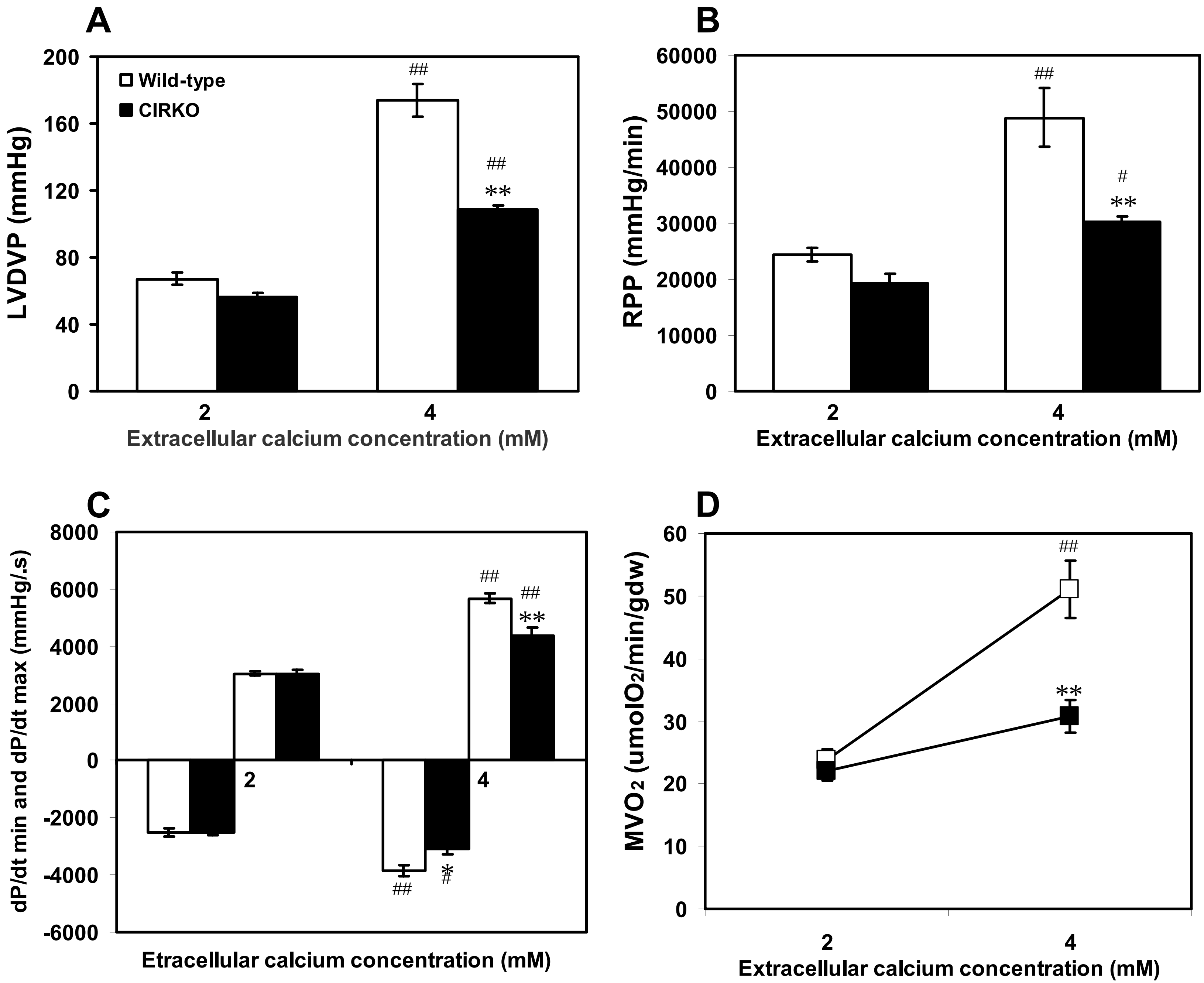

SUPPLEMENTAL FIGURE S3

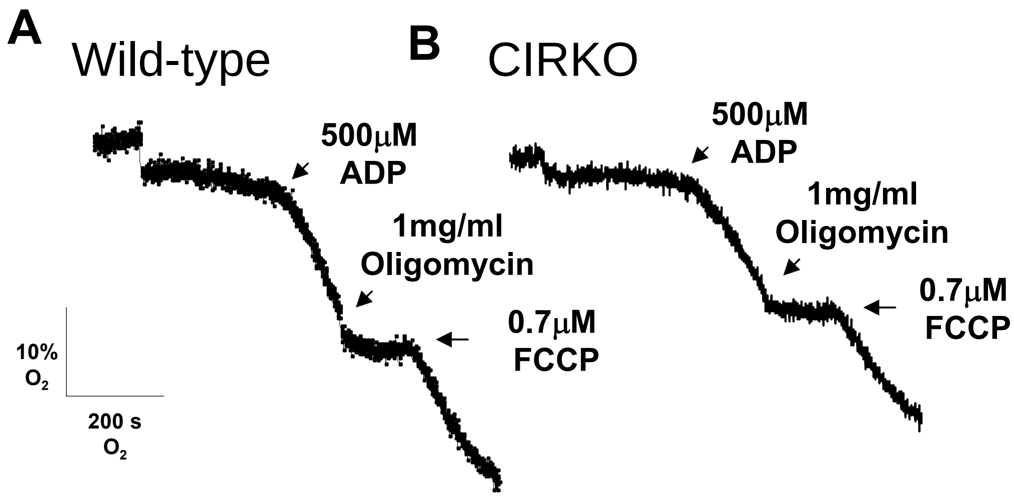

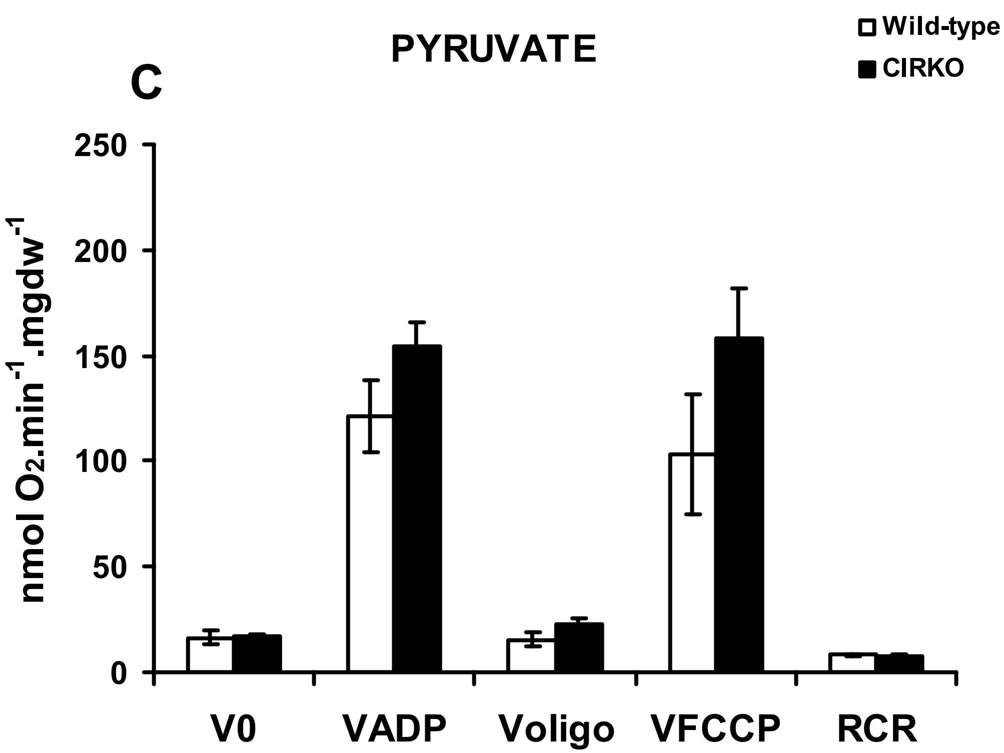

SUPPLEMENTAL FIGURE S4

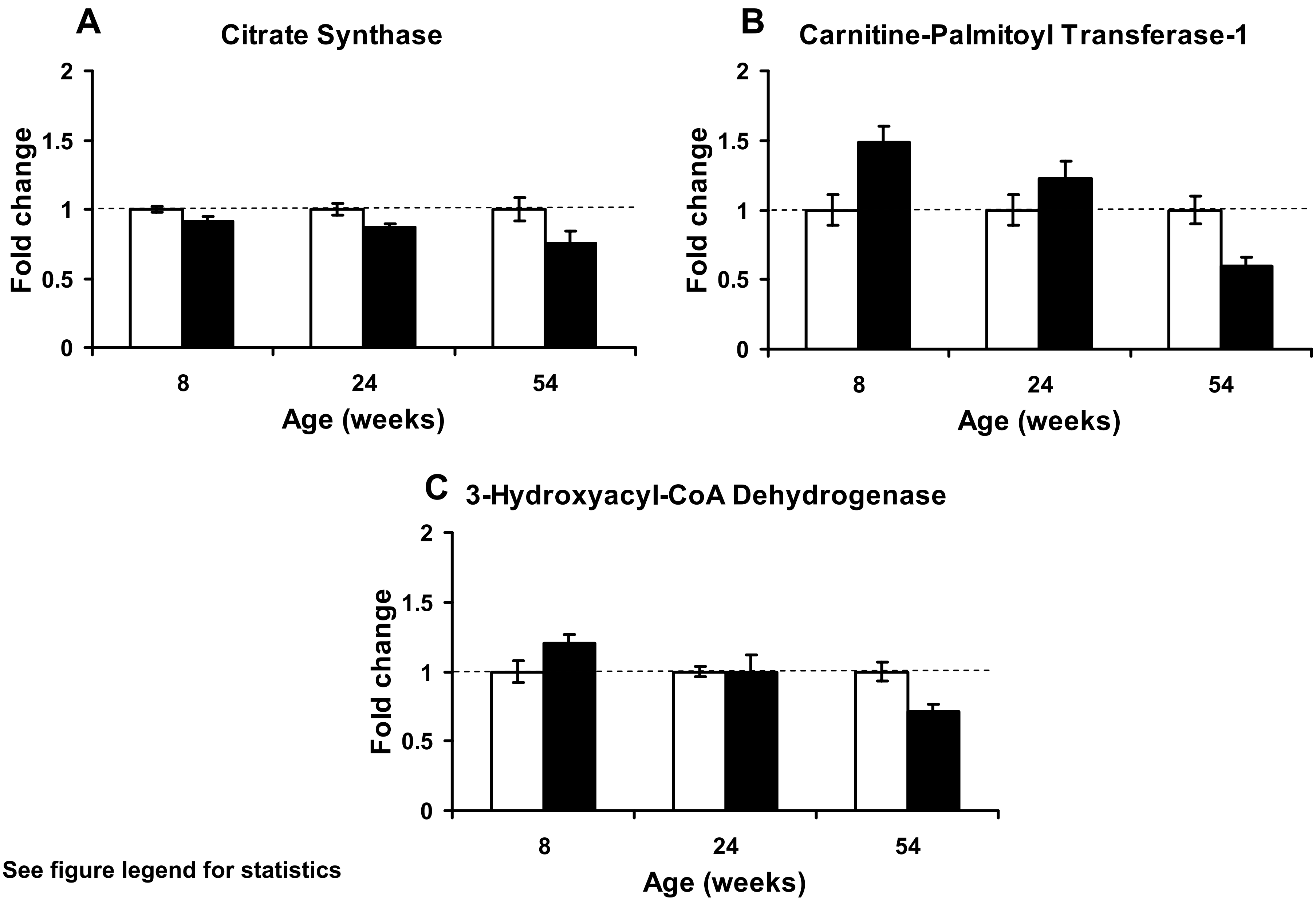

See figure legend for statistics

SUPPLEMENTAL FIGURE S5

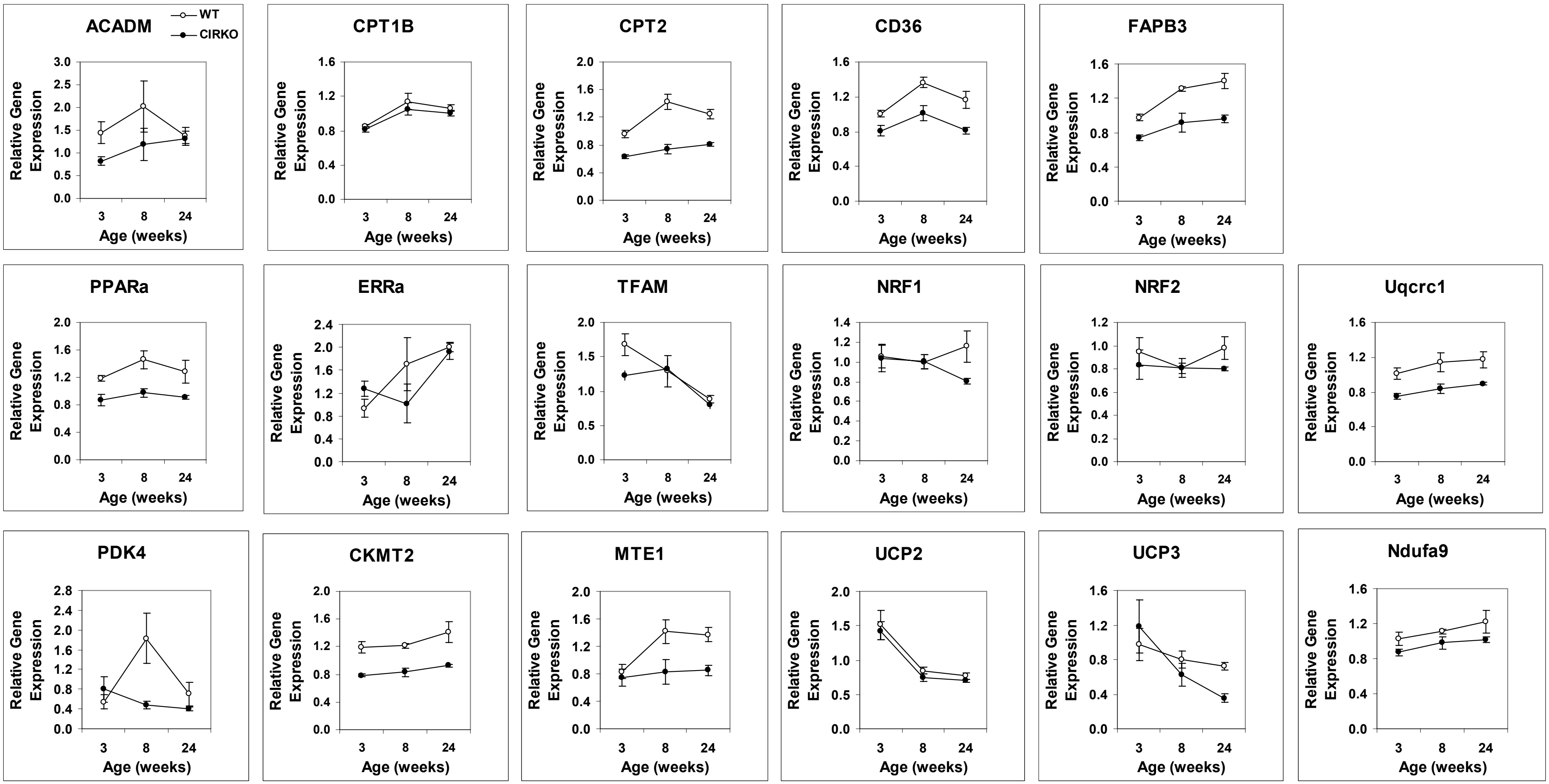

SUPPLEMENTAL FIGURE S6

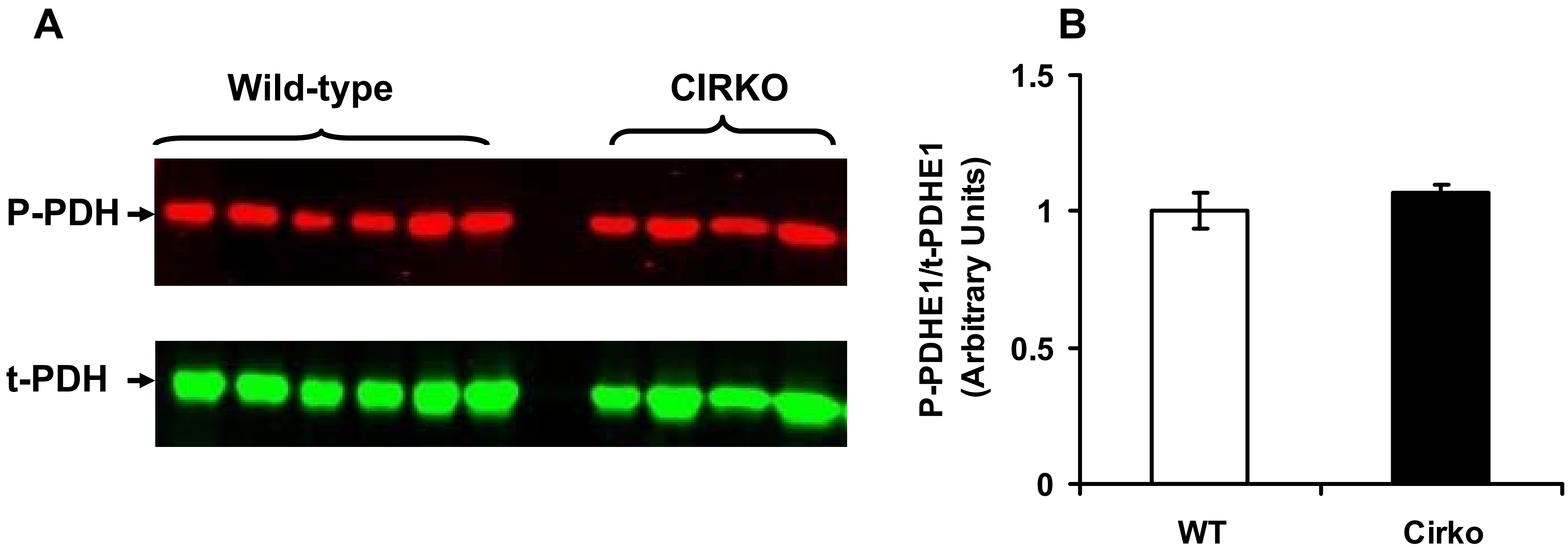

SUPPLEMENTAL FIGURE S7

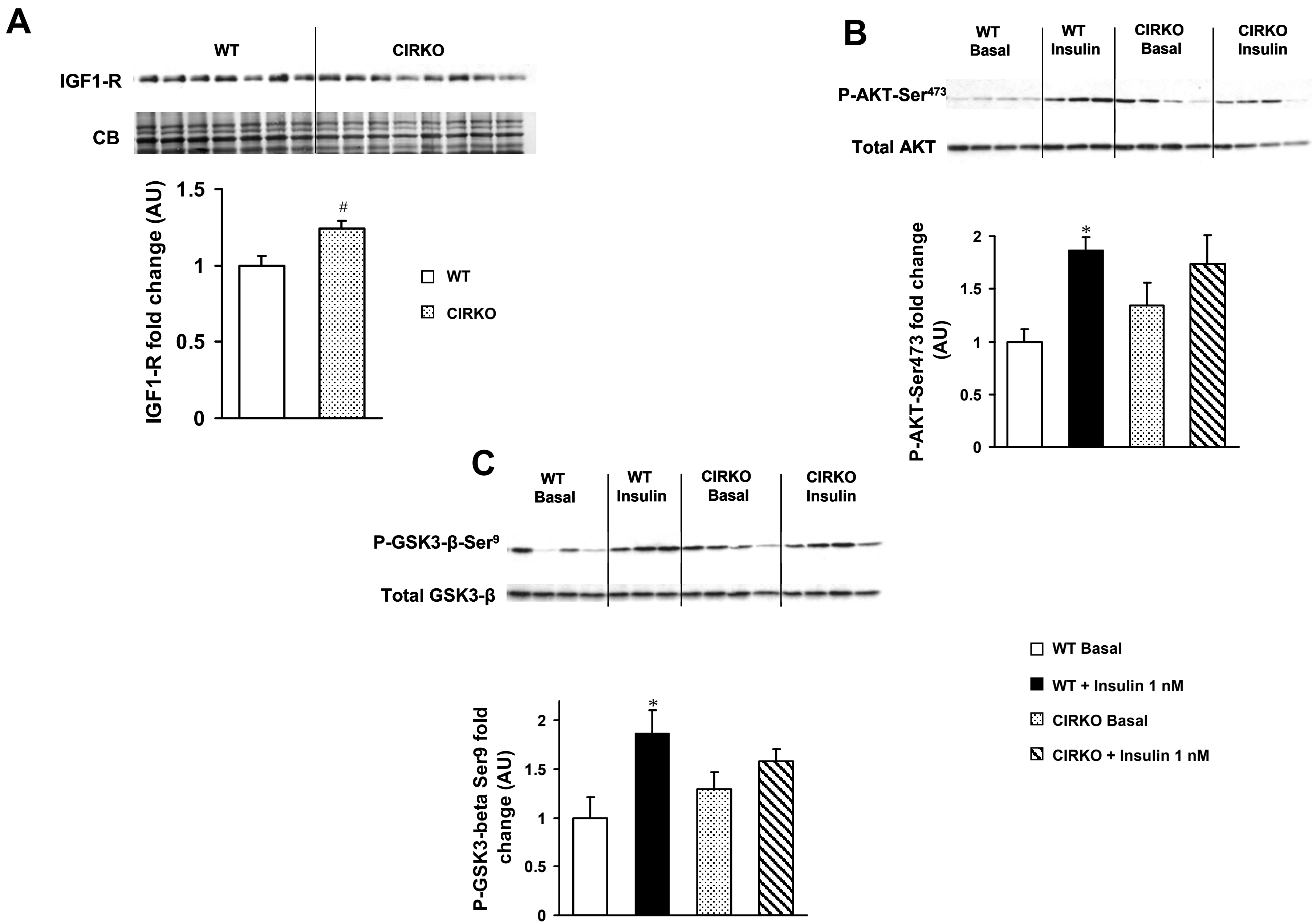

SUPPLEMENTAL FIGURE S8

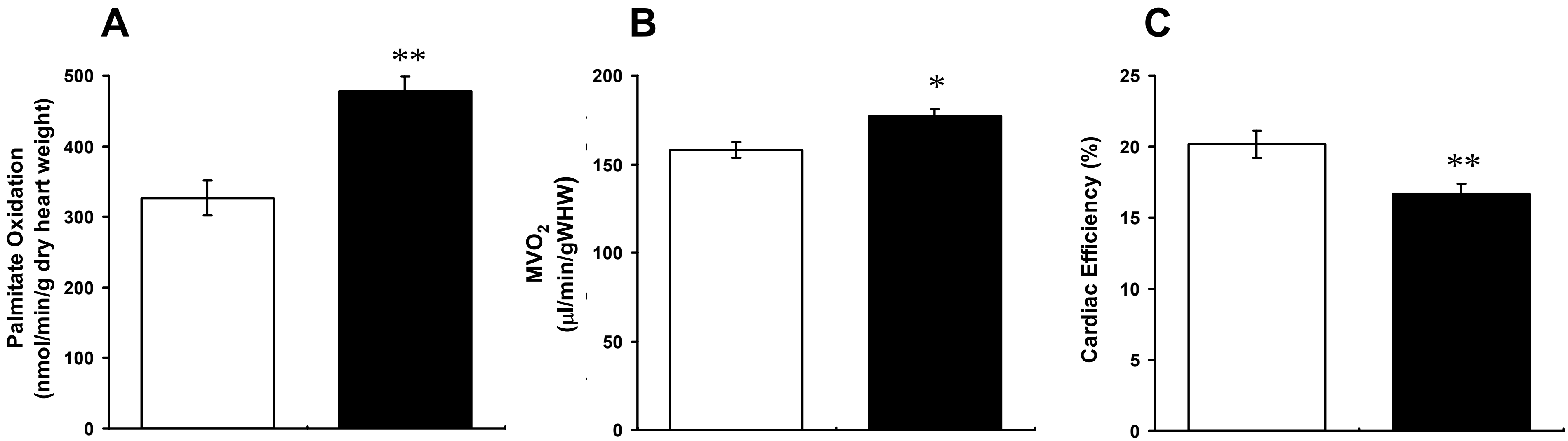

REFERENCES

1. Zerbetto E, Vergani L, Dabbeni-Sala F. Quantification of muscle mitochondrial oxidative phosphorylation enzymes via histochemical staining of blue native polyacrylamide gels. *Electrophoresis.* 1997;18:2059-2064.

2. Silva JC, Denny R, Dorschel CA, Gorenstein M, Kass IJ, Li GZ, McKenna T, Nold MJ, Richardson K, Young P, Geromanos S. Quantitative proteomic analysis by accurate mass retention time pairs. *Analytical chemistry.* 2005;77:2187-2200.

3. Boudina S, Sena S, O'Neill BT, Tathireddy P, Young ME, Abel ED. Reduced mitochondrial oxidative capacity and increased mitochondrial uncoupling impair myocardial energetics in obesity. *Circulation.* 2005;112:2686-2695.

4. Yan LJ, Levine RL, Sohal RS. Oxidative damage during aging targets mitochondrial aconitase. *Proc Natl Acad Sci U S A.* 1997;94:11168-11172.